NAVIER–STOKES ENTROPY CONTROLLED COMBUSTION INSTABILITY ANALYSIS FOR LIQUID PROPELLANTS

T.J. Chung* and W.S. Yoon**
Department of Mechanical Engineering
The University of Alabama in Huntsville
Huntsville, AL 35899, USA

ABSTRACT

Navier–Stokes solutions are used to calculate oscillatory components of pressure, velocity, and density, which in turn provide necessary data to compute energy growth factors to determine combustion instability. It is shown that wave instabilities are associated with changes in entropy and the space and time averages of oscillatory components of pressure, velocity and density, together with the mean flow field in the energy equation. Compressible laminar and turbulent flows and reacting flows with hydrogen/oxygen combustion are considered in this paper. The space shuttle main engine combustion/thrust chamber is used for illustration of the theory. The analysis shows that the increase of mean pressure and disturbances consistently results in the increase in instability. It is shown that adequate combustion instability analysis requires at least third order nonlinearity in energy growth or decay.

1. INTRODUCTION

It is well known that growth or decay of energy is responsible for instability or stability of waves in fluids, respectively. We recognize that there are three different sources of energy growth or decay. They are: (1) pressure fluctuations (acoustic waves); (2) velocity fluctuations (hydrodynamic waves due to transition to turbulence, shear layers, or shedding of vortices); and (3) density fluctuations (intrinsic waves due to compressibility and/or chain reactions of unstable chemical radicals in combustion). Extensive research works have been carried out for acoustic instability [1–6] and hydrodynamic instability [6–9], with limited studies available on intrinsic instability [10]. Flandro [11] presented the energy balance method in which the acoustic energy equation was used to develop the nonlinear stability equation based on isentropic assumption and linear superposition of entropy change. Each of the above types of instability requires different methods of analyses and unification of such methods has not been attempted. The objective of the present paper is directed toward our desire to introduce a unified general method for wave instability analyses.

The basic approach toward this achievement, called the entropy controlled instability (ECI) method, is founded on the concept of entropy changes in which nonlinearity is a prime factor. This is because our ultimate goal is a general theory which enables nonlinear waves to be studied in detail without making simplified initial assumptions such as isentropy. Nonlinear waves invoke nonisentropy in which growth or decay of energy is properly accounted for. This line of thinking is

---

* Professor
** Graduate Research Assistant

dictated also by our desire to deal with both incompressible and compressible fluids, with the general approach being capable of handling compressible or reacting flows and a special case reduced to incompressible flows. To this end, we examine the energy equation written in terms of entropy changes as well as fluctuations of pressure, velocity, and density. Introducing spatial averages, or applying the Green—Gauss theorem, we integrate the energy equation by parts through which boundary surface integrals arise, playing the role of acoustic intensities. Additional terms representing the spatial growth of energy also arise in this process of integration by parts. Performing the time averages, we finally arrive at the nonlinear, nonisentropic stability equation, which assumes the form of nonlinear integro—ordinary differential equation for the energy growth factor indicative of stability or instability of waves. The integrands of this nonlinear stability equation (the word 'nonisentropic' omitted but implied hereafter) are contributed from the results of the Navier—Stokes solutions using the Taylor—Galerkin finite elements [12—16]. The nonlinear stability equation will then be solved using the fourth order Runge—Kutta method to calculate the energy growth factor. It is shown that the general theory presented here is reduced to a simple linear theory of Cantrell and Hart [1] or Culick [2] as a special case with appropriate assumptions.

We shall discuss the details of these processes in the following sections.

2. ENTROPY CONTROLLED INSTABILITY (ECI) METHOD

2.1 Navier—Stokes Solutions

In order to perform stability analysis, it is necessary to first solve the unsteady Navier—Stokes equations representing the desired physics. To this end, the most general conservation form of Navier Stokes equations for compressible flows is written as

$$\frac{\partial \mathbf{U}}{\partial t} + \frac{\partial \mathbf{F}_j}{\partial x_j} + \frac{\partial \mathbf{G}_j}{\partial x_j} = \mathbf{B} \tag{1}$$

where

$$\mathbf{U} = \begin{bmatrix} \rho \\ \rho v_i \\ \rho E \\ \rho Y_k \end{bmatrix} \quad \mathbf{F}_j = \begin{bmatrix} \rho v_j \\ \rho v_i v_j + p\delta_{ij} \\ \rho E v_j + p v_j \\ \rho Y_k v_j \end{bmatrix} \tag{1a,b}$$

$$\mathbf{G}_j = \begin{bmatrix} 0 \\ -\tau_{ij} \\ -\tau_{ij} v_i + q_j \\ \rho D Y_{k,j} \end{bmatrix} \quad \mathbf{B} = \begin{bmatrix} 0 \\ \rho \sum_{k=1}^{N} Y_k f_{ki} \\ \rho \sum_{k=1}^{N} Y_k f_{ki} v_i \\ w_k \end{bmatrix} \tag{1c,d}$$

where τ_{ij} is the viscous stress tensor

$$\tau_{ij} = \mu \left(v_{i,j} + v_{j,i} - \frac{2}{3} v_{k,k} \delta_{ij} \right) \tag{1e}$$

and E is the stagnation energy

$$E = e + \frac{1}{2} v_i v_i = c_p T - \frac{p}{\rho} + \frac{1}{2} v_i v_i \tag{1f}$$

and f_{ki} is the body force and q_j is the heat flux vector.

$$q_j = -\lambda T_{,j} + \rho D \sum_{k=1}^{N} H_k Y_{k,j} \tag{1g}$$

Here, λ and D are the thermal conductivity and mass diffusivity, respectively. H_k is the total enthalpy of species k, Y_k is the mass fraction for the species k, and w_k is the reaction rate for the species k. Note that all derivatives are covariant in case of cylindrical coordinates.

For turbulent flows we add to (1) additional transport equations for turbulent kinetic energy and dissipation energy (k—ϵ model), respectively,

$$\frac{\partial}{\partial t}\left(\rho k\right) + \frac{\partial}{\partial x_j}\left(\rho v_j k - \mu_k \frac{\partial k}{\partial x_j}\right) = G - \rho\epsilon \tag{1h}$$

$$\frac{\partial}{\partial \rho}\left(\rho \epsilon\right) + \frac{\partial}{\partial x_j}\left(\rho v_j \epsilon - \mu_\epsilon \frac{\partial \epsilon}{\partial x_j}\right) = c_1 \frac{\epsilon}{k} G - c_2 \rho \epsilon^2 / k \tag{1i}$$

where G is the turbulent thermal dissipation energy transport and

$$\mu_k = \mu + \frac{\mu_t}{\sigma_k}, \qquad \mu_\epsilon = \mu + \frac{\mu_t}{\sigma_\epsilon}, \qquad \mu_t = \rho c_\mu \frac{k^2}{\epsilon},$$

$$c_\mu = 0.09, \qquad c_1 = 1.44, \qquad c_2 = 1.92, \qquad \sigma_k = 1.0, \qquad \sigma_\epsilon = 1.3$$

Appropriate modifications to the equations of momentum and energy and the suitable turbulent combustion model should be included as detailed in [12].

The solution procedure using the Taylor—Galerkin method are found in [13—17], which will not be repeated here. The space shuttle main engine combustion/thrust chamber is used for numerical analysis. Examples include shock waves interacting with laminar and turbulent flows and with laminar reacting flows. Calculations of energy growth factors and stability criteria are discussed below.

2.2 Nonlinear, Nonisentropic Stability Analysis

With the solutions of unsteady Navier—Stokes equations for the time—dependent periodic oscillatory initial boundary conditions available, we now turn to the entropy controlled instability (ECI) method of determining the unstable wave phenomena. To introduce entropy changes in the energy equation, we begin with thermodynamic relations for an ideal nonisentropic gas and write the pressure gradients in terms of density and entropy gradients,

$$p_{,i} = a^2 \rho_{,i} + \frac{\rho a^2}{c_p} S_{,i} \tag{2}$$

where a is the speed of sound, S is the specific entropy, and the comma denotes the partial derivative with respect to x_i. The gradient of the stagnation energy, E, assumes the form

$$E_{,i} = \left(c_p T - \frac{p}{\rho} + \tfrac{1}{2} v_j v_j\right)_{,i} \tag{3}$$

where the repeated indices imply summing. Performing the differentiation implied in (2) results in

$$E_{,i} = \frac{c_v}{R\rho} p_{,i} - \frac{c_v}{R} \frac{p}{\rho^2} \rho_{,i} + v_j v_{j,i} \tag{4}$$

where R is the specific gas constant. Substituting (2) into (4) yields

$$\rho E_{,i} = \frac{p}{\rho} \rho_{,i} + \frac{p}{R} S_{,i} + \rho\, v_j v_{j,i} \tag{5}$$

Let us now examine the conservation form of the energy equation

$$\frac{\partial}{\partial t}\left(\rho E\right) + \left(\rho E\, v_i - \sigma_{ij}\, v_j\right)_{,i} = 0 \tag{6}$$

where σ_{ij} is the stress tensor

$$\sigma_{ij} = p\delta_{ij} + \mu\left(v_{i,j} + v_{j,i} - \frac{2}{3} v_{k,k}\, \delta_{ij}\right) \tag{7}$$

Substituting (5) into (6) gives

$$\frac{\partial}{\partial t}\left(\rho E\right) + E\left(\rho\, v_i\right)_{,i} + v_i\left[\frac{p}{\rho}\rho_{,i} + \frac{p}{R} S_{,i} + \rho v_j v_{j,i}\right] - \left(\sigma_{ij} v_j\right)_{,i} = 0 \tag{8}$$

This is the entropy controlled energy equation, instrumental in determining the nonlinear wave instability.

The pressure, velocity, and density may be written in the form

$$p = \bar{p} + p' \tag{9a}$$

$$v_i = \bar{v}_i + v_i' \tag{9b}$$

$$\rho = \bar{\rho} + \rho' \tag{9c}$$

where the symbols, bar and prime, denote the mean and fluctuation parts, respectively. From thermodynamic relations we may write the entropy difference in the form

$$S - S_0 = R\ell n\left[\left(1 + \frac{p'}{\bar{p}}\right)^{\frac{1}{\gamma-1}} \left(1 + \frac{\rho'}{\bar{\rho}}\right)^{-\frac{\gamma}{\gamma-1}}\right] \tag{10}$$

Expanding the RHS of (10) in infinite series and after some algebra, we obtain

$$S = R\left[S_{(1)} + S_{(2)} + S_{(3)} + S_{(4)} + \ldots\right] + S_0 \tag{11}$$

where S_0 is the entropy at the initial state ($S_0 = 0$), and

$$S_{(1)} = \frac{1}{\gamma-1}\frac{p'}{\bar{p}} - \frac{\gamma}{\gamma-1}\frac{\rho'}{\bar{\rho}}$$

$$S_{(2)} = -\frac{1}{2}\left[\frac{1}{\gamma-1}\left(\frac{p'}{\bar{p}}\right)^2 - \frac{\gamma}{\gamma-1}\left(\frac{\rho'}{\bar{\rho}}\right)^2\right]$$

$$S_{(3)} = \frac{1}{3}\left[\frac{1}{\gamma-1}\left(\frac{p'}{\bar{p}}\right)^3 - \frac{\gamma}{\gamma-1}\left(\frac{\rho'}{\bar{\rho}}\right)^3\right]$$

$$S_{(4)} = -\frac{1}{4}\left[\frac{1}{\gamma-1}\left(\frac{p'}{p}\right)^4 - \frac{\gamma}{\gamma-1}\left(\frac{\rho'}{\rho}\right)^4\right]$$

Here the terms with fifth order or higher are neglected, assuming that they are negligible.

To obtain acoustic energy equation, we apply the Green—Gauss theorem or integrate (8) by parts and take a time average in the form

$$\left\langle \int_\Omega \frac{\partial}{\partial t}(\rho E)\, d\Omega + \int_\Gamma \left[E\rho v_i n_i + v_i\left(p\, n_i + \frac{p}{R} S\, n_i + \rho\, v_j v_j\, n_i\right) - \sigma_{ij} v_j\, n_i\right] d\Gamma - \int_\Omega \left[E_{,i}\, \rho v_i \right.\right.$$

$$\left.\left. + \rho\left(v_i \frac{p}{\rho}\right)_{,i} + \left(v_i \frac{p}{R}\right)_{,i} S + \left(\rho v_i v_j\right)_{,i} v_j\right] d\Omega \right\rangle = 0 \qquad (12)$$

where Ω and Γ represent the domain and boundary surface, respectively, $\langle \cdot \rangle$ implies time averages and n_i denotes the component of a vector normal to the surface. It is interesting to note that the domain integral terms (last four terms) arise as a result of the integration by parts implying the spatial growth of energy. This spatial growth of energy is in addition to the usual temporal growth of energy indicated by the domain integral with the time derivative (first term in (8)). Let ϵ be the energy growth factor, stable for $0 \leq \epsilon \leq 1$, unstable for $\epsilon > 1$, with $\epsilon=1$ indicating the neutral stability. The fluctuation terms in (9) and (11) contribute to (12) as multiples of higher order fluctuations. Multiplying the like powers of ϵ with the fluctuation terms of the same order and retaining the terms up to and including the fourth order, we obtain

$$\left\langle \int (\cdot)\, d\Omega \right\rangle = \left\langle \int_\Omega \left(\delta_0 + \epsilon\delta_1 + \epsilon^2\delta_2 + \epsilon^3\delta_3 + \epsilon^4\delta_4 + \ldots\right) d\Omega \right\rangle \qquad (13a)$$

$$\left\langle \int_\Gamma (\cdot)\, d\Gamma \right\rangle = \left\langle \int_\Gamma \left(\phi_0 + \epsilon\phi_1 + \epsilon^2\phi_2 + \epsilon^3\phi_3 + \epsilon^4\phi_4 + \ldots\right) d\Gamma \right\rangle \qquad (13b)$$

Here δ_0 and ϕ_0 contain only the mean quantity, δ_1, δ_2, δ_3, δ_4 and ϕ_1, ϕ_2, ϕ_3, ϕ_4 are referred to as the first, second, third, and fourth order perturbations capable of growth and decay in acoustic energy as dictated by the magnitudes of ϵ, growing if $\epsilon > 1$ and decaying if $\epsilon < 1$. Notice that the relations in (9a, b, and c) imply that the Navier—Stokes solutions are obtained with the initial condition $\epsilon = 1$ and the energy in (13) may grow or decay in accordance with the magnitude of ϵ from the initial or reference state $\epsilon = 1$.

Performing the differentiation as implied in (12), we obtain

$$\frac{\partial}{\partial t}\left(\epsilon^2 E_1 + \epsilon^3 E_2 + \epsilon^4 E_3\right) = \epsilon^2 I_1 + \epsilon^3 I_2 + \epsilon^4 I_3 \qquad (14)$$

in which the zeroth order terms are canceled and first order terms vanish due to time averages. Notice that the time averages are contained in $E_{(i)}$ and $I_{(i)}$. Here, the energy growth factor ϵ is an explicit function of time. However, $E_{(i)}$ is no longer an explicit function of time because of its time averages. Thus the partial derivative with respect to time in (14) involves only ϵ, not $E_{(i)}$, so that

$$\frac{d\epsilon}{dt} = \frac{\epsilon^2 I_1 + \epsilon^3 I_2 + \epsilon^4 I_3}{2\epsilon E_1 + 3\epsilon^2 E_2 + 4\epsilon^3 E_3}$$

or

$$\frac{d\epsilon}{dt} = \left(\epsilon I_1 + \epsilon^2 I_2 + \epsilon^3 I_3\right) \frac{1}{2E_1} \left\{1 - \epsilon \frac{3E_2}{2E_1} + \epsilon^2 \left[\frac{9}{4}\left(\frac{E_2}{E_1}\right) - \frac{2E_3}{E_1}\right]\right\} \tag{15}$$

where higher order terms and those terms much smaller than unity have been neglected.

It follows from (15) that the nonlinear stability equation takes the form

$$\frac{d\epsilon}{dt} - a_1\epsilon - a_2\epsilon^2 - a_3\epsilon^3 = 0 \tag{16}$$

This is a form identical to Flandro [11], although the basic approach to the formulation and the solution procedures differ. Here a_1, a_2, and a_3 are energy growth rate parameters of first, second, and third order, respectively.

$$a_1 = \frac{1}{2E_1} I_1 \tag{17a}$$

$$a_2 = \frac{1}{2E_1}\left(I_2 - \frac{3E_2}{2E_1} I_1\right) \tag{17b}$$

$$a_3 = \frac{1}{2E_1}\left\{I_3 - \frac{3E_2}{2E_1} I_2 + \left[\frac{9}{4}\left(\frac{E_2}{E_1}\right)^2 - \frac{2E_3}{E_1}\right] I_1\right\} \tag{17c}$$

with

$$E_1 = \left\langle \int_\Omega a^{(1)}\, d\Omega \right\rangle \tag{18a}$$

$$E_2 = \left\langle \int_\Omega a^{(2)}\, d\Omega \right\rangle \tag{18b}$$

$$E_3 = \left\langle \int_\Omega a^{(3)}\, d\Omega \right\rangle \tag{18c}$$

$$I_1 = \left\langle \int_\Omega b^{(1)}\, d\Omega \right\rangle - \left\langle \int_\Gamma c_i^{(1)}\, n_i\, d\Gamma \right\rangle \tag{19a}$$

$$I_2 = \left\langle \int_\Omega b^{(2)}\, d\Omega \right\rangle - \left\langle \int_\Gamma c_i^{(2)}\, n_i\, d\Gamma \right\rangle \tag{19b}$$

$$I_3 = \left\langle \int_\Omega b^{(3)}\, d\Omega \right\rangle - \left\langle \int_\Gamma c_i^{(3)}\, n_i\, d\Gamma \right\rangle \tag{19c}$$

Explicit forms of $a^{(1)}$, $b^{(1)}$, and $c^{(1)}$ will be discussed in Section 3 and the integrands for the second and third order growth parameters are shown in Appendix A. The physical significance and interpretations of the above process will be discussed in the following subsection.

2.3 Physical Interpretation

The physical significance in the above development may be schematically demonstrated as shown in Fig. 1. First, unsteady Navier–Stokes solutions with time dependent oscillatory initial boundary conditions are obtained at each computational grid as shown in Fig. 1a. A typical variable vs time, (Fig. 1b), at any grid point (finite element node) may exhibit sawtooth type wave forms as well as sinusoidal waves. Imagine that several variables at each of the several thousand nodes present themselves in the form as shown in Fig. 1b. Each wave form of different

frequencies at different spatial locations is expected to contribute to the overall stability or instability. Take one complete peak wave form period as indicated by $\tau = n\Delta t$ where Δt is the Navier—Stokes time step with n usually being in the range between teens and hundreds.

Performing the time average for this time period ($n\Delta t$), we obtain the mean quantity ($\bar{f}$) of the variable f. Then the disturbance (fluctuation) part f ' is calculated as

$$f' = f - \bar{f}$$

where f is the Navier—Stokes solution.

From these data, spatial integrations involving both domain and boundary surfaces and time averages (Fig. 1a) as dictated by (18) and (19) are then carried out.
Here, $\int_\Omega a^{(n)} d\Omega$ denotes the temporal growth of energy, whereas $\int_\Omega b^{(n)} d\Omega$ represents the spatial growth of energy. The boundary integral $\int_\Gamma c_i^{(n)} n_i \, d\Gamma$ indicates the acoustic intensity. For combustion chamber applications, the burning surface admittance, response functions, or information on nozzle entrance or acoustic liner, etc., can be initially imposed on the Navier—Stokes solutions as boundary conditions to generate the oscillatory motions as depicted in Fig. 1b. These boundary data, however, reappear as called for in the integrand, $c_i^{(n)}$, in (19). They act as acoustic intensity and eventually contribute to the determination of stability or instability of the system.

The ingredients of $a^{(n)}$, $b^{(n)}$, and $c_i^{(n)}$ arise from fluctuation parts of the Navier—Stokes solutions as well as the mean parts. These fluctuations through the temporal growth of energy $a^{(n)}$, spatial growth of energy $b^{(n)}$, and acoustic intensity $c_i^{(n)}$, are responsible for driving the system toward instability. The consequences lead to determination of the energy growth factor vs time as shown in Fig. 1c by solving the nonlinear stability equation (16). It is important to realize that the Navier—Stokes solutions and the nonlinear stability equation (16) encompass acoustic waves, hydrodynamic (vortical or shear layer) waves, intrinsic (density fluctuations or chemically reacting combustion) waves, or combined effects of all types of wave interactions.

Notice that, in (6) and (12), heat flux changes are not directly involved. This is because the spatial integration of fluctuations of heat flux or temperature vanishes upon time averages. However, fluctuations of temperature and chemical species mass fractions have been included in the Navier—Stokes solutions of (1), thus indirectly contributing to the fluctuations of density (ρ') in the stability calculations.

Some comments on the mean pressure changes (DC shifts), pressure coupling, velocity coupling, limit cycles, and triggering are in order. These phenomena often observed in solid propellant combustion chambers, would appear in the flowfield under appropriate initial and boundary conditions during the Navier—Stokes calculations. The purpose of the ECI method is merely to determine whether the flowfield containing such physical phenomena is stable or unstable. It is emphasized that all physical phenomena are expected to prevail and be identified in the solution of Navier—Stokes equations, which are then reconfirmed in the stability analysis.

3. LINEAR INSTABILITY

To gain an insight into the solution of (16), we may neglect the last two terms associated

with the second and third order energy growth rate parameters and write

$$\frac{d\epsilon}{dt} - a_1\epsilon = 0 \tag{20}$$

which yields a solution in the form

$$\ln \epsilon = a_1 t + c_1 \tag{21}$$

To establish an initial condition, we assume neutral stability $\epsilon = 1$ at $t = 0$. This gives $c_1 = 0$. Thus, the solution takes the form

$$\epsilon = e^{a_1 t} \tag{22}$$

Under this initial condition, there exists a unique solution for any given a_1 with $t > 0$. The stability criteria are:

Stable: $0 \leq \epsilon \leq 1$ with $-\infty < a_1 < 0$

Neutral stability: $\epsilon = 1$ with $a_1 = 0$

Unstable: $1 < \epsilon \leq \infty$ with $0 < a_1 < \infty$

Although these criteria are not applicable for the nonlinear equation (16) when a_2 and a_3 are involved, the same initial condition, $\epsilon_1 = 1$ at $t = 0$, as originally defined in (13a, b), can be used. That is, there exists a unique solution ϵ for any given a_1, a_2 and a_3 with $t > 0$. Therefore, the criteria for stability in terms of ϵ remain the same with various combinations of a_1, a_2, and a_3.

3.1 Nonisentropic case

Notice that the integration involved in the growth rate parameters a_1, a_2, and a_3 and the subsequent solution of the nonlinear ordinary differential equation (16) are formidable. However, it would be informative to examine the case of linear instability ($a_2 = 0$, $a_3 = 0$) given by (20) but with nonisentropy. Therefore, the first order energy growth rate parameter takes the form, from (20) and (17a),

$$a_1 = \frac{1}{\epsilon}\frac{d\epsilon}{dt} = \frac{I_1}{2E_1} = \frac{\left\langle \int_\Omega b^{(1)} d\Omega \right\rangle - \left\langle \int_\Omega c_i^{(1)}\, n_i d\Gamma \right\rangle}{\left\langle 2 \int a^{(1)}\, d\Omega \right\rangle} \tag{23}$$

Assuming that the fluid is inviscid ($\mu = 0$) the explicit forms of integrals in (23) become

$$\int_\Omega a^{(1)}\, d\Omega = \int_\Omega \left(\frac{\bar\rho}{2} v_j' v_j' + \rho' \bar v_j v_j' \right) d\Omega \tag{24a}$$

$$\int_\Omega b^{(1)}\, d\Omega = \int_\Omega \left\{ \bar\rho \bar v_i \left(-\frac{p'\rho'}{(\gamma-1)\bar\rho^2} + \frac{\bar p \rho'^2}{(\gamma-1)\bar\rho^3} + \frac{1}{2} v_j' v_j' \right)_{,i} + \left(\bar\rho v_i' + \bar v_i \rho' \right) \left(\frac{p'}{(\gamma-1)\bar\rho} \right.\right.$$

$$\left. - \frac{\bar p\, \rho'}{(\gamma-1)\bar\rho^2} + \bar v_j v_j' \right)_{,i} + v_i' \rho' \left(\frac{\bar p}{(\gamma-1)\bar\rho} + \frac{1}{2} \bar v_j \bar v_j \right)_{,i} + \bar\rho \left(-\frac{\bar v_i p' \rho'}{\bar\rho^2} + \frac{\bar v_i \bar p}{\bar\rho^3} \rho'^2 \right.$$

$$\left.\left. + \frac{p' v_i'}{\bar\rho} - \frac{\bar p v_i' \rho'}{\bar\rho^2} \right)_{,i} + \rho' \left(\frac{\bar v_i p'}{\bar\rho} - \frac{\bar p \bar v_i \rho'}{\bar\rho^2} + \frac{\bar p v_i'}{\bar\rho} \right)_{,i} + \left(\frac{p'}{(\gamma-1)\bar p} - \frac{\gamma\rho'}{(\gamma-1)\bar\rho} \right) \left(\bar p v_i' \right.$$

$$+ p'\bar{v}_i\big)_{,i} + \Big(-\frac{p'^2}{2(\gamma-1)\bar{p}^2} + \frac{\gamma\rho'^2}{2(\gamma-1)\bar{\rho}^2}\Big)\big(\bar{p}\bar{v}_i\big)_{,i} + \bar{v}_j\left(\bar{\rho}v_i'v_j' + \rho'\bar{v}_jv_i' + \rho'\bar{v}_iv_j'\right)_{,i}$$

$$+ v_j'\left(\bar{\rho}\bar{v}_iv_j' + \bar{\rho}\,v_i'\bar{v}_j + \rho'\bar{v}_i\bar{v}_j\right)_{,i} \tag{24b}$$

$$\int_\Gamma c_i^{(1)}n_i d\Gamma = \int_\Gamma\Big\{\bar{\rho}\bar{v}_i\Big(-\frac{p'\rho'}{(\gamma-1)\bar{\rho}^2} + \frac{\bar{p}\rho'^2}{(\gamma-1)\bar{\rho}^3} + \frac{1}{2}v_j'v_j'\Big) + \big(\bar{\rho}\,v_i' + \bar{v}_i\rho'\big)\Big(\frac{p'}{(\gamma-1)\bar{\rho}}$$

$$-\frac{\bar{p}\rho'}{(\gamma-1)\bar{\rho}^2} + \bar{v}_jv_j'\Big) + \rho'v_i'\Big(\frac{\bar{p}}{(\gamma-1)\bar{\rho}} + \frac{1}{2}\bar{v}_j\bar{v}_j\Big) + p'v_i' + \Big(-\frac{p'^2}{2(\gamma-1)\bar{\rho}^2}$$

$$+\frac{\gamma\rho'^2}{2(\gamma-1)\bar{\rho}^2}\Big)\bar{p}\bar{v}_i + \Big(\frac{p'}{(\gamma-1)\bar{p}} - \frac{\gamma\rho'}{(\gamma-1)\bar{\rho}}\Big)\big(\bar{p}v_i' + p'\bar{v}_i\big) + \bar{v}_i\left(\bar{\rho}v_j'v_j' + 2\rho'\bar{v}_jv_j'\right)$$

$$+ v_i'\left(2\bar{\rho}\bar{v}_iv_i' + \rho'\bar{v}_i\bar{v}_i\right) + v_i'\,p'\Big\}\,n_i\,d\Gamma \tag{24c}$$

Notice that the first term on RHS of (24a) represents the kinetic energy of the sound wave. If isentropic assumption is made, then ρ' can be expanded into infinite series in terms of p', p'^2, ... such that the second term on the RHS of (24a) contains the potential energy of the sound wave usually identified in the linear acoustic energy equation. However, our objective here is to allow entropy to change and, therefore, we must keep ρ' to remain subjected to nonisentropy. Another important observation is the domain integral for $b^{(1)}$ which has appeared for the first time as a result of the integration by parts (24b), signifying the spatial growth of energy. The boundary integral for $c_i^{(1)}n_i$ contains the terms of acoustic intensity normally identified in the linear acoustics, but significantly in a different form. Additional terms which arise in the process developed in this analysis will allow determination of stability or instability of wave motions with explicit changes of entropy contributing to the growth or decay of energy. However, it is not possible to evaluate the integrals (24a, b, c) because the density fluctuations ρ' cannot analytically be determined. This difficulty can be resolved in a certain special case if isentropy is assumed as discussed below.

3.2 Isentropic case

If the flow is isentropic then it can be shown that

$$\rho' = \frac{p'}{\bar{a}^2} + \frac{1}{2}\bar{\rho}\,\frac{1-\gamma}{\gamma^2}\frac{p'^2}{\bar{p}^2} + \frac{1}{6}\frac{\bar{\rho}(1-\gamma)(1-2\gamma)}{\gamma^3}\frac{p'^3}{\bar{p}^3} + \frac{1}{24}\frac{\bar{\rho}(1-\gamma)(1-2\gamma)(1-3\gamma)}{\gamma^4}\frac{p'^4}{\bar{p}^4} + \cdots \tag{25}$$

where $\bar{a}$ denotes the speed of sound without flow. As far as the linear stability is concerned only the first two terms on the RHS of (25) will contribute to (24a, b, c) as seen from substitution of (25) into (9c) and subsequently to (24a,b,c).

$$\int_\Omega a^{(1)}\,d\Omega = \int_\Omega\Big(\frac{\bar{\rho}}{2}v_j'v_j' + \frac{p'^2}{2\bar{\rho}\bar{a}^2} + \frac{\bar{v}_jv_j'p'}{\bar{a}^2}\Big)\,d\Omega \tag{26a}$$

$$\int_\Omega b^{(1)}\,d\Omega = \int_\Omega \left\{\bar{\rho}\bar{v}_i\left(\frac{p'^2}{(\gamma-1)\bar{\rho}^2\bar{a}^2} + \frac{\bar{p}p'^2}{(\gamma-1)\bar{\rho}^3\bar{a}^4} + \frac{1}{2}v_j'v_j' + \ldots\right)_{,i} + \ldots\right\} d\Omega \tag{26b}$$

$$\int_\Gamma c_i^{(1)} n_i d\Gamma = \int_\Gamma \left\{p'v_i' + \frac{p'^2\bar{v}_i}{\bar{\rho}\bar{a}^2} + \bar{\rho}\,v_i'\bar{v}_j v_j' + \frac{p'\bar{v}_i\bar{v}_j v_j'}{\bar{a}^2} + \ldots\right\} n_i d\Gamma \tag{26c}$$

Since ρ' does not appear in the integrals of (26a, b, c) it is now possible to substitute analytical forms of p' and v_i' in terms of time dependent acoustic eigenfunctions and perform explicit analytical integrations. However, it is clear that the additional domain integral (26b) and many more additional terms arising as a result of the entropy controlled energy equation given by (8) or (12) will produce the results quite contrary to the traditional isentropic solution, (see Cantrell and Hart [1] or Culick [2])

$$\alpha_1 = \frac{-\left\langle \int_\Gamma \left[p'v_i' + \frac{p'^2\bar{v}_i}{\bar{\rho}\bar{a}^2} + \bar{\rho}\,v_i'\bar{v}_j v_j' + \frac{p'\bar{v}_i\bar{v}_j v_j'}{\bar{a}^2}\right] n_i d\Gamma\right\rangle}{2\left\langle \int_\Omega \left(\frac{1}{2}\bar{\rho}\,v_j'v_j' + \frac{p'^2}{2\bar{\rho}\bar{a}^2} + \frac{\bar{v}_j v_j' p'}{\bar{a}^2}\right) d\Omega\right\rangle} \tag{27}$$

Note that the terms on the numerator are the same as the first four terms of (26c) with the negative sign as indicated in (19a), and the terms of the denominator are identical to those in (26a). However, the domain integral of (26b) is absent. This integral contributed by $b^{(1)}$ represents the spatial growth or decay of energy as balanced by the boundary conditions and acoustic intensities on the boundary surface. This is in contrast to the temporal growth or decay of energy originating from (26a).

Despite the special feature in the proposed formulation, however, the analytical forms for p' and v_i' as used by Cantrell and Hart [1], are incapable of simulating sawtooth type shock waves. For example consider the acoustic field of a cylinder with the radius R and length L,

$$p' = \mathfrak{Re}\left[\bar{p}\cos\frac{\ell\pi x}{L}\,J_m\left(\beta_{mn}\frac{r}{R}\right)\cos(m\theta)\,e^{i\omega t}\right] \tag{28a}$$

$$v_i' = \mathfrak{Re}\left[\frac{i\bar{p}}{\omega\bar{\rho}}\cos\frac{\ell\pi x}{L}\,J_m(\beta_{mn}\frac{r}{R})\cos(m\theta)\,e^{i\omega t}\right] \tag{28b}$$

Here angular frequency, ω, is defined as

$$\omega = \bar{a}\left[\left(\frac{\ell\pi}{L}\right)^2 + \left(\frac{\beta_{mn}}{R}\right)\right]^{\frac{1}{2}}$$

with ℓ, m, n, being the positive integers or zero, J_{mn} the Bessel function of order m, and β_{mn} the nth root of $J'_{mn}(\beta) = 0$. Retaining only those terms arising from the standard acoustic energy equations (without employing the entropy controlled energy equation), a simple solution can be obtained using (28a, b) to calculate the linear energy growth rate parameter α_1 as demonstrated by Cantrell and Hart [1]. If the entire terms implied in (26a, b, c) are used, however, it is no longer possible to obtain analytical solutions.

4. NONLINEAR, NONISENTROPIC INSTABILITY

Nonlinear, nonisentropic waves occur in many industrial propulsion combustion systems. Shock waves may interact with turbulent vortical waves or shear layers of liquid jets in gas medium. Density fluctuations due to chemical reactions may also be combined. We have seen that analytical solutions of even the linear instability by ECI method presented in the previous section are intractable. First of all, the fluctuation variables p', v_i', and ρ' are to be numerically calculated by solving the Navier–Stokes equations. Then we must perform numerical integrations required to evaluate the energy growth rate parameters a_1, a_2, and a_3. Subsequently, numerical solutions of the nonlinear ordinary differential equation must be carried out.

Numerical integrations as required by (18a, b, c) and (19a, b, c) can be performed most efficiently by Galerkin finite element techniques to calculate the energy growth rate parameters a_1, a_2, and a_3 according to (17a, b, c). Finally the nonlinear ordinally differential equation (16) is solved using the Newton–Raphson method to determine the energy growth factor ϵ. Thus, it is seen that the determination of stability $(0 < \epsilon < 1)$, instability $(\epsilon > 1)$, or neutral stability $(\epsilon = 1)$ is made available for each $n\Delta t$ period and we move on until desired time is reached as shown in Fig. 1c. It is interesting to see that, in this decision making process of stability or instability, "all" nodal points (thousands of nodes) with their nodal values of "all" variables have participated. Every wave peak, whether sinusoidal or sawtooth type, has been recognized. Shock waves interacting with turbulence, shear layers, or shedding of vortices, or effects of chemical reactions can be reflected in calculations of (17 a, b, c) and could have eventually contributed to the solution of (16) for determination of stability or instability.

Solutions to the nonlinear ordinary differential equation (16) may be obtained using the fourth–order Runge–Kutta method. Iterations will continue until convergence.

5. SOLUTION PROCEDURE

It is clear that the solution consists of three parts. First the Navier–Stokes equations are solved. Then the results of the Navier–Stokes solutions are used to calculate the energy growth rate parameters. Finally the energy growth factor is computed by solving the nonlinear, nonisentropic stability equation. Step–by–step solution procedures are described as follows:

(1) With appropriate boundary and initial conditions, solve the Navier–Stokes equations. Initially, the mean pressure, $\bar{p}$, and temperature, T, based on the ideal gas law, are specified everywhere. At the inlet, however, the oscillatory pressure is input $[p = \bar{p}\ (1 + d \sin \omega t)]$, where d is the % disturbance and ω is the frequency.

(2) Calculate p, v_i, ρ, and T. Taylor–Galerkin finite element method with adaptive meshes is used in Navier–Stokes solutions.

(3) Advance time steps (Δt) of Navier–Stokes solutions to obtain wave oscillations to cover at least one wave period. Δt is determined continuously which satisfies an acceptable Courant number.

(4) Take time averages for the period $n\Delta t$ with n chosen such that at least one peak wave

period is covered. These time averages lead to $\bar{p}$, $\bar{v}_i$, and $\bar{\rho}$.

(5) Calculate the fluctuation quantities as $p' = p - \bar{p}$, $v_i' = v_i - \bar{v}_i$, $\rho' = \rho - \bar{\rho}$, where p, v_i, and ρ represent Navier–Stokes solutions.

(6) Calculate the energy growth rate parameters α_1, α_2, and α_3 from (17a, b, c) using the results of step 5, above.

(7) Solve the nonlinear differential equation (16) using the Newton–Raphson method with the initial condition $\epsilon = 1$ at $t = 0$, corresponding to neutral stability.

(8) Repeat steps 1 through 7 until the desired length of time has been advanced.

Note that for each time–average period in step 4, above, instability and stability are determined by $\epsilon > 1$ and $\epsilon < 1$, respectively, with $\epsilon = 1$ being the neutral stability. If the system is found to be unstable, it is not necessary to proceed to the next time step. However, for the entire ranges of time for which Navier–Stokes solutions are available, the stability analysis may be performed, even if instability has been found in previous time steps. This is so because Navier–Stokes solutions are independent of the stability analysis as formulated here. Rather, the stability analysis here determines the state of stability or instability based on current flowfield as calculated from the Navier–Stokes solution. The following applications are based on computer code ECI–2.

6. APPLICATIONS

To illustrate the theory, an axisymmetric geometry of combustion/thrust chamber is investigated for various types of flow: Case 1, laminar compressible nonreacting flows; Case 2, turbulent compressible nonreacting flows, and Case 3, chemically reacting laminar compressible flows with hydrogen/oxygen combustion.

Case 1 Laminar Compressible Nonreacting Flows

Figure 2a shows the axisymmetric geometry of combustion/thrust chamber with 965 triangular elements and 528 nodes as a consequence of adaptive mesh process. Notice that in the vicinity of the walls approximately 80% of the nodes are concentrated resulting in prominent boundary layers. To demonstrate the capability of the code, initially, the steady state flow field without disturbances is examined. The velocity vectors and contours of Mach number, pressure, and temperature are shown in Fig. 2b, c, d, and e, respectively. Formation of boundary layers (Fig. 2b), separation of boundary layers and weak shock waves downstream (Fig. 2c, d), and decrease of temperature downstream and toward the wall (Fig. 2e) are evident.

With disturbances of d = 10%, 20% and 30% imposed on the mean pressures at the inlet, the Navier–Stokes transient analyses are performed. The time steps are continuously adjusted to satisfy acceptable Courant numbers, $0.2 \leq CN \leq 0.4$, for convergence. The graphical representation of oscillations of all variables at every node versus time is overwhelmingly complex. Therefore, wave forms only for d = 30% and $\bar{p}$ = 3000 psi at three selected positions, A at (1.8, 11.43 cm), B at (31.75, 11.43 cm), and C at (63.5, 6.55 cm) are shown in Fig. 3. Note that, although the sinusoidal input is provided at the inlet, the oscillations downstream become nonlinear, possibly of sawtooth type.

In Fig. 4, the energy growth factors ϵ for $\bar{p} = 500$ psi are shown for various % disturbances. It is seen that for d = 10%, the energy growth factor remains in the stable region $\epsilon < 1$. The dotted lines and solid lines indicate the results for the linear (Eq. 20) and nonlinear (16) cases, respectively. As the disturbance increases (d = 20%) the energy growth factor reaches the neutral stability, $\epsilon = 1$ at $t \simeq 0.015$ sec. For d = 30%, the energy growth factor increases further ($\epsilon = 1.038$) at $t \simeq 0.2$ sec. Notice that the linear analysis underestimates the stability if stable whereas it underestimates the instability if unstable. The general trend is that instability is proportional to the percent disturbances.

As the mean pressure increases ($\bar{p} = 3000$ psi), the possibility of instability increases as shown in Fig. 5, with the conclusion that instability is proportional to the mean pressure. Recall that for d = 10%, $\bar{p} = 500$ psi, stability prevailed throughout whereas with d = 10%, $\bar{p} = 3000$ psi neutral stability has been reached. The peak values of ϵ for $\bar{p} = 3000$ psi are significantly larger than those for $\bar{p} = 500$ psi.

Case 2 Turbulent Compressible Nonreacting Flows

The discretized geometry for a steady state turbulent compressible nonreacting flow is shown in Fig. 6a with a total of 2688 elements and 1416 nodes. As seen in Fig. 6b (velocity vectors) and Fig. 6c (Mach number contours), the boundary layers are thinner than in the case of laminar flow, leading to turbulent shock wave interactions. It is clear that gradients of pressure (Fig. 6d) and temperature (Fig. 6e) are larger than in the case of laminar flow.

Wave forms of transient turbulent nonreacting flow with disturbances, d = 30%, $\bar{p} = 3000$ psi, at the three positions are shown in Fig. 7. Although the wave forms in turbulence at these positions do not seem much different from the case of laminar flow, it is quite possible that wave forms at other locations where turbulent velocity gradients are significant would be drastically changed in contrast to the laminar flow.

The energy growth factors for turbulent flow are shown in Fig. 8 for $\bar{p} = 500$ psi and Fig. 9 for $\bar{p} = 3000$ psi. It is interesting to see that the effect of turbulence is to increase instability as compared with the laminar flow. The general trend other than the turbulent effect, however, remains the same as the laminar flow. That is, instability is proportional to disturbances and the mean pressure. The linear analysis again shows that stability is underestimated if stable and instability is underestimated if unstable.

Case 3 Chemically Reacting Laminar Compressible Flows with Hydrogen/Oxygen Combustion

Figure 10 shows the discretized geometry for a steady state chemically reacting flow without disturbances. A total of 1580 elements and 844 nodes are used. The chemical reactions considered are shown in Appendix B. The mass fractions at the inlet are 0.111 for H_2 and 0.889 for O_2, and the inlet velocity is 500 m/s. In this analysis the effect of viscosity is ignored to ensure an enhanced computational convergence, which leads to a flow without boundary layers along the wall. Due to the finite rate chemistry and stiffness arising from the chemical source terms, the computational convergence is rather slow. In the region of chemical reactions the velocity is decreased (Fig. 10b) and the Mach number contours are spaced widely apart (Fig. 10c), resulting in a rapid increase of pressure (Fig. 10d), but no evidence of shock discontinuities (Fig. 10c, d) between the throat and the downstream nozzle area. Temperature increases in the region of combustion in a sharp contrast to the nonreacting cases (Fig. 2e and Fig. 6e).

The contours of 8 species are shown in Fig. 11, beginning with the reactants, hydrogen (Fig. 11a) and oxygen (Fig. 11b), followed by products, H (Fig. 11c), HO_2 (Fig. 11d), H_2O (Fig. 11e), H_2O_2 (Fig. 11f), O (Fig. 11g), and OH (Fig. 11h). It is observed that H_2 is depleted halfway between the inlet and throat whereas O_2 prevails further downstream before it is depleted behind the throat. Most of the products (including the radicals), H, HO_2, O, and OH rapidly increase from the inlet and become maximum as they pass through the throat. In contrast, H_2O and H_2O_2 gradually increase downstream with a constant rate.

Figure 12 shows the wave forms of the transient chemically reacting flow with disturbances, d = 30% and $\bar{p}$ = 500 psi, at the three positions considered earlier. Notice that, with chemical reactions, the frequencies of waves are very low and the response is quite slow particularly at downstream locations. Once again, the results plotted in Fig. 12 are misleading because oscillations in other locations (over 800 nodes) may prove to be significantly different. After all, combustion instability is determined by the stability equation, not by the appearance of oscillations observed at random locations.

In Fig. 13, the energy growth factors for the chemically reacting flow are examined. First of all, the linear analysis (dotted line) shows an apparent faulty prediction of instability for d = 10%, in which the nonlinear analysis indicates $\epsilon \simeq 0$ throughout the time segment investigated. Obviously, this is an indication of unreliability of the linear analysis. For d = 20%, however, the linear analysis appears to give the consistent results similar to the earlier examples in that the linear analysis underestimates the stability when stable and underestimates the instability when unstable. The nonlinear analysis shows that, for d = 20% and d = 30%, the peak values of energy growth factors are significantly larger than the nonreacting cases. Does this imply that chemically reacting flows always tend toward instability? An affirmative answer to this question is premature. In fact the entire investigation presented here is subject to the future verification by experimental measurements.

7. CONCLUSIONS

The entropy controlled instability method has been applied to various problems in laminar flows, turbulent flows, and reacting flows for determination of stability conditions. The following conclusions are reached:

(1) Instability increases with an increase of disturbances.

(2) Instability increases with an increase of the mean pressure.

(3) Instability increases as laminar flows are changed to turbulent flows.

(4) Instability due to production of radicals under the finite rate chemistry is significant for the case investigated.

(5) The linear stability analysis underestimates stability if stable and underestimates instability if unstable.

(6) The correct stability analysis calls for at least the third order nonlinearity.

(7) Future studies are required to validate the present theory in comparison with experimental results for those cases other than examined in this paper.

C-4

ACKNOWLEDGEMENT: This research was supported in part by the US Army Missile Command (DAAH01—87—D—0021) and in part by NASA/MSFC (NAS8—36955).

REFERENCES

1. Cantrell, R.H., and Hart, R.W., "Interaction Between Sound and Flow in Acoustic Cavities: Mass, Momentum, and Energy Considerations," Journal of Acous. Soc. Amer., Vol. 36, No. 4, pp. 697—706, 1964.

2. Culick, F.E.C., "Stability of Three—Dimensional Motions in a Combustion Chamber," Combustion Science and Technology, Vol. 10, pp. 109—124, 1975.

3. Sirignano, W.A., and Crocco, L., "A Shock Wave Model of Unstable Rocket Combustion," AIAA Journal, Vol. 2, No. 7, p. 1285, July 1964.

4. Harvje, D.T., and Reardon, F.H., Ed., "Liquid Propellant Rocket Combustion Instability," NASA SP—194, 1972.

5. Baum, J.D., and Levine, J.N., "Modeling of Nonlinear Combustion Instability in Solid Propellant Rocket Motors," AFRPL TR—83—058, February 1984.

6. Chung, T.J., and Sohn, J.L., "Interactions of Coupled Acoustic and Vortical Instability," AIAA Journal, Vol. 24, No. 10, pp. 1582—1595, 1982.

7. Michalke, A., "On the Inviscid Instability of the Hyperbolic Tangent Velocity Profiles," Journal of Fluid Mechanics, Vol. 9, pp. 543—556, 1964.

8. Michalke, A., "Vortex Formation in a Free Boundary Layer According to Stability Theory," Journal of Fluid Mechanics, Vol. 22, Pt. 2, 1965.

9. Michalke, A., "On Spatially Growing Disturbances in an Inviscid Shear Layer," Journal of Fluid Mechanics, Vol. 25, Pt. 4, pp. 521—554, 1966.

10. Williams, F.A., "Combustion Theory," The Benjamin/Cummings Publishing Co., 2nd Ed., 1985.

11. Flandro, G.A., "Energy Balance Analysis of Nonlinear Combustion Instability," AIAA Journal of Propulsion, Vol. 1, No. 3, pp. 210—221, 1985.

12. Kim, Y.M., and Chung, T.J., "Finite Element Analysis of Turbulent Diffusion Flames," AIAA Journal, Vol. 27, No. 3, pp 330—339, 1989.

13. Spradley, L.W., Stalnaker, J.F., and LÖhner, R., "Finite Element Code for Combustion Analysis of Advanced Propulsion Systems," Final Report, SBIR, NAS8—38022, 1989.

14. Yoon, W.S., Chung, T.J., Stalnaker, J.F., and Spradley, L.W., "Analysis of Unstable Nonlinear Combustion Waves Using Entropy Controlled Instability (ECI) Method", AIAA paper, AIAA90—2362, July 1990.

15. Donea, J., "A Taylor—Galerkin Method for Convective Transport Problems", Int. J. Num. Meth. Engng., 20, pp. 101—119, 1984.

16. LÖhner, R., "A Finite Element Solver for Axisymmetric Compressible Flows", AIAA Paper 89—1794, June 12—14, 1989.

17. Chung, T.J., Finite Element Analysis in Fluids and Heat Transfer, Krieger Publishing Company, 1991.

APPENDIX A

INTEGRANDS OF E_1, E_2, E_3, I_1, I_2, I_3

$$a^{(1)} = \frac{\bar{\rho}}{2} v_j' v_j' + \rho' \bar{v}_j v_j'$$

$$a^{(2)} = \frac{1}{2} \rho' v_j' v_j'$$

$$a^{(3)} = -\frac{1}{\gamma-1} \left(\frac{\bar{p}\rho'^4}{\bar{\rho}^4}\right)$$

$$b^{(1)} = \bar{\rho}\bar{v}_i \left(-\frac{p'\rho'}{(\gamma-1)\bar{\rho}^2} + \frac{\bar{p}\,\rho'^2}{(\gamma-1)\bar{\rho}^3} + \frac{1}{2} v_j' v_j'\right)_{,i} + (\bar{\rho} v_i' + \bar{v}_i \rho')\left(\frac{p'}{(\gamma-1)\bar{\rho}} - \frac{\bar{p}\rho'}{(\gamma-1)\bar{\rho}^2}\right.$$

$$\left. + \bar{v}_j v_j'\right)_{,i} + v_i' \rho' \left(\frac{\bar{p}}{(\gamma-1)\bar{\rho}} + \frac{1}{2} \bar{v}_j \bar{v}_j\right)_{,i} + \bar{\rho}\left(-\frac{\bar{v}_i p' \rho'}{\bar{\rho}^2} + \frac{\bar{v}_i \bar{p}}{\bar{\rho}^3} \rho'^2 + \frac{p' v_i'}{\bar{\rho}} - \frac{\bar{p} v_i' \rho'}{\bar{\rho}^2}\right)_{,i}$$

$$+ \rho'\left(\frac{\bar{v}_i p'}{\bar{\rho}} - \frac{\bar{p}\bar{v}_i \rho'}{\bar{\rho}^2} + \frac{\bar{p} v_i'}{\bar{\rho}}\right)_{,i} + \left(-\frac{p'^2}{2(\gamma-1)\bar{p}^2} + \frac{\gamma\rho'^2}{2(\gamma-1)\bar{\rho}^2}\right)(\bar{p}\bar{v}_i)_{,i} + \left(\frac{p'}{(\gamma-1)\bar{p}} - \frac{\gamma\rho'}{(\gamma-1)\bar{\rho}}\right)$$

$$(\bar{p} v_i' + p' \bar{v}_i)_{,i} + \bar{v}_j \left(\bar{\rho} v_i' v_j' + \rho' \bar{v}_j v_i' + \rho' \bar{v}_i v_j'\right)_{,i} + v_j' \left(\bar{\rho}\bar{v}_i v_j' + \bar{\rho} v_i' \bar{v}_j + \rho' \bar{v}_i \bar{v}_j\right)_{,i}$$

$$b^{(2)} = (\bar{\rho} v_i' + \bar{v}_i \rho')\left(-\frac{p'\rho'}{(\gamma-1)\bar{\rho}^2} + \frac{\bar{p}\rho'^2}{(\gamma-1)\bar{\rho}^3} + \frac{1}{2} v_j' v_j'\right)_{,i} + \rho' v_i' \left(\frac{p'}{(\gamma-1)\bar{\rho}} - \frac{\bar{p}\rho'}{(\gamma-1)\bar{\rho}^2}\right.$$

$$\left. + \bar{v}_j v_j'\right)_{,i} + \bar{\rho}\bar{v}_i \left(\frac{p'\rho'^2}{(\gamma-1)\bar{\rho}^3} - \frac{\bar{p}\rho'^3}{(\gamma-1)\bar{\rho}^4}\right)_{,i} + \bar{\rho}\left(\frac{\bar{v}_i p' \rho'^2}{\bar{\rho}^3} - \frac{\bar{v}_i \bar{p}\rho'^3}{\bar{\rho}^4} - \frac{v_i' p' \rho'}{\bar{\rho}^2} + \frac{\bar{p} v_i' \rho'^2}{\bar{\rho}^3}\right)_{,i}$$

$$+ \rho'\left(-\frac{\bar{v}_i p' \rho'}{\bar{\rho}^2} + \frac{\bar{v}_i \bar{p}\rho'^2}{\bar{\rho}^3} + \frac{p' v_i'}{\bar{\rho}} - \frac{\bar{p} v_i' \rho'}{\bar{\rho}^2}\right)_{,i} + \left(\frac{p'^3}{3(\gamma-1)\bar{p}^3} - \frac{\gamma\rho'^3}{3(\gamma-1)\bar{\rho}^3}\right)(\bar{p}\bar{v}_i)_{,i}$$

$$+ \left(-\frac{p'^2}{2(\gamma-1)\bar{p}^2} + \frac{\gamma\rho'^2}{2(\gamma-1)\bar{\rho}^2}\right)(\bar{p} v_i' + p' \bar{v}_i)_{,i} + \left(\frac{p'}{(\gamma-1)\bar{p}} - \frac{\gamma\rho'}{(\gamma-1)\bar{\rho}}\right)(p' v_i')_{,i}$$

$$+ \bar{v}_j \left(\rho' v_i' v_j'\right)_{,i} + v_j' \left(\bar{\rho} v_i' v_j' + \bar{v}_i \rho' v_j' + \bar{v}_j \rho' v_i'\right)_{,i}$$

$$b^{(3)} = \bar{\rho}\bar{v}_i \left(-\frac{p'\rho'^3}{(\gamma-1)\bar{\rho}^4}\right)_{,i} + (\bar{\rho} v_i' + \bar{v}_i \rho')\left(\frac{p'\rho'^2}{(\gamma-1)\bar{\rho}^3} - \frac{\bar{p}\rho'^3}{(\gamma-1)\bar{\rho}^4}\right)_{,i} + \rho' v_i' \left(-\frac{p'\rho'}{(\gamma-1)\bar{\rho}^2} + \frac{\bar{p}\rho'^2}{(\gamma-1)\bar{\rho}^3}\right.$$

$$+\frac{1}{2}\,v_j'v_j')_{,i}+\bar{\rho}\left(\frac{v_i'p'\rho'^2}{\bar{\rho}^3}-\frac{\bar{p}v_i'\rho'^3}{\bar{\rho}^4}-\frac{\bar{v}_ip'\rho'^3}{\bar{\rho}^4}\right)+\rho'\left(\frac{\bar{v}_ip'\rho'^2}{\bar{\rho}^3}-\frac{\bar{p}\bar{v}_i\rho'^3}{\bar{\rho}^4}-\frac{v_i'p'\rho'}{\bar{\rho}^2}+\frac{\bar{p}v_i'\rho'^2}{\bar{\rho}^3}\right)_{,i}$$

$$+\left(\bar{p}\bar{v}_i\right)_{,i}\left(-\frac{p'^4}{4(\gamma-1)\bar{p}^4}+\frac{\gamma\rho'^4}{4(\gamma-1)\bar{\rho}^4}\right)+\left(\bar{p}v_i'+p'\bar{v}_i\right)_{,i}\left(\frac{p'^3}{3(\gamma-1)\bar{p}^3}-\frac{\gamma\rho'^3}{6(\gamma-1)\bar{\rho}^3}\right)$$

$$+(p'v_i')_{,i}\left(-\frac{p'^2}{2(\gamma-1)\bar{p}^2}+\frac{\gamma\rho'^2}{2(\gamma-1)\bar{\rho}^2}\right)+\left(\rho'v_i'v_j'\right)_{,i}v_j'$$

$$c_i^{(1)}=\bar{\rho}\bar{v}_i\left(-\frac{p'\rho'}{(\gamma-1)\bar{\rho}^2}+\frac{\bar{p}\rho'^2}{(\gamma-1)\bar{\rho}^3}+\frac{1}{2}\,v_j'v_j'\right)+\left(\bar{\rho}v_i'+\bar{v}_i\rho'\right)\left(\frac{p'}{(\gamma-1)\bar{\rho}}-\frac{\bar{p}\rho'}{(\gamma-1)\bar{\rho}^2}+\bar{v}_jv_j'\right)$$

$$\rho'v_i'\left(\frac{\bar{p}}{(\gamma-1)\bar{\rho}}+\frac{1}{2}\,\bar{v}_j\bar{v}_j\right)+p'v_i'+\left(-\frac{p'^2}{2(\gamma-1)\bar{p}^2}+\frac{\gamma\rho'^2}{2(\gamma-1)\bar{\rho}^2}\right)\bar{p}\bar{v}_i+\left(\frac{p'}{(\gamma-1)\bar{p}}-\frac{\gamma\rho'}{(\gamma-1)\bar{\rho}}\right)$$

$$\left(\bar{p}v_i'+p'\bar{v}_i\right)+\bar{v}_i\left(\bar{\rho}v_j'v_j'+2\rho'\bar{v}_jv_j'\right)+v_i'\left(2\bar{\rho}\bar{v}_jv_j'+\rho'\bar{v}_j\bar{v}_j\right)+v_j'\left[p'\delta_{ij}-\mu\left(v_{i,j}'\right.\right.$$

$$\left.\left.+v_{j,i}'\right)\right]+\frac{2}{3}\,\mu\,v_{k,k}'v_i'$$

$$c_i^{(2)}=\left(\bar{\rho}v_i'+\bar{v}_i\rho'\right)\left(-\frac{p'\rho'}{(\gamma-1)\bar{\rho}^2}+\frac{\bar{p}\rho'^2}{(\gamma-1)\bar{\rho}^3}+\frac{1}{2}\,v_j'v_j'\right)+\rho'v_i'\left(\frac{p'}{(\gamma-1)\bar{\rho}}-\frac{\bar{p}\rho'}{(\gamma-1)\bar{\rho}^2}\right.$$

$$\left.+\bar{v}_jv_j'\right)+\bar{\rho}\bar{v}_i\left(\frac{p'\rho'^2}{(\gamma-1)\bar{\rho}^3}-\frac{\bar{p}\,\rho'^3}{(\gamma-1)\bar{\rho}^4}\right)+\left(\frac{p'^3}{3(\gamma-1)\bar{p}^3}-\frac{\gamma\rho'^3}{3(\gamma-1)\bar{\rho}^3}\right)\bar{p}\bar{v}_i+\left(\frac{p'^2}{2(\gamma-1)\bar{p}^2}\right.$$

$$\left.-\frac{\gamma\rho'^2}{2(\gamma-1)\bar{\rho}^2}\right)\left(\bar{p}v_i'+p'\bar{v}_i\right)+\left(\frac{p'}{(\gamma-1)\bar{p}}-\frac{\gamma\rho'}{(\gamma-1)\bar{\rho}}\right)p'v_i'+\rho'\bar{v}_iv_j'v_j'+\bar{\rho}v_i'v_j'v_j'+2\rho'v_i'\bar{v}_jv_j'$$

$$c_i^{(3)}=\bar{\rho}\bar{v}_i\left(-\frac{p'\rho'^3}{(\gamma-1)\bar{\rho}^4}\right)+\left(\bar{\rho}v_i'+\bar{v}_i\rho'\right)\left(\frac{p'\rho'^2}{(\gamma-1)\bar{\rho}^3}-\frac{\bar{p}\rho'^3}{(\gamma-1)\bar{\rho}^4}\right)+\rho'v_i'\left(-\frac{p'\rho'}{(\gamma-1)\bar{\rho}^2}+\frac{\bar{p}\rho'^2}{(\gamma-1)\bar{\rho}^3}\right.$$

$$\left.+\frac{1}{2}\,v_j'v_j'\right)+\left(\frac{p'^3}{3(\gamma-1)\bar{p}^3}-\frac{\gamma\rho'^3}{3(\gamma-1)\bar{\rho}^3}\right)\left(\bar{p}v_i'+p'\bar{v}_i\right)+\left(-\frac{p'^2}{2(\gamma-1)\bar{p}^2}+\frac{\gamma\rho'^2}{2(\gamma-1)\bar{\rho}^2}\right)p'v_i'$$

$$+\left(-\frac{p'^4}{4(\gamma-1)\bar{p}^4}+\frac{\gamma\rho'^4}{4(\gamma-1)\bar{\rho}^4}\right)\bar{p}\bar{v}_i+\rho'v_i'v_j'v_j'$$

APPENDIX B

REACTION EQUATIONS

$H_2 + O_2 = 2OH$

$H + O_2 = OH + O$

$OH + H_2 = H_2O + H$

$O + H_2 = OH + H$

$2OH = H_2O + O$

$H + OH + M = H_2O + M$

$2H + M = H_2 + M$

$H + O_2 + M = HO_2 + M$

$HO_2 + OH = H_2O + O_2$

$HO_2 + H = H_2 + O_2$

$HO_2 + H = 2OH$

$HO_2 + O = OH + O_2$

$2HO_2 = H_2O_2 + O_2$

$HO_2 + H_2 = H_2O_2 + H$

$H_2O_2 + OH = HO_2 + H_2O$

$H_2O_2 + H = OH + HO_2$

$H_2O_2 + O = OH + HO_2$

$H_2O_2 + M = 2OH + M$

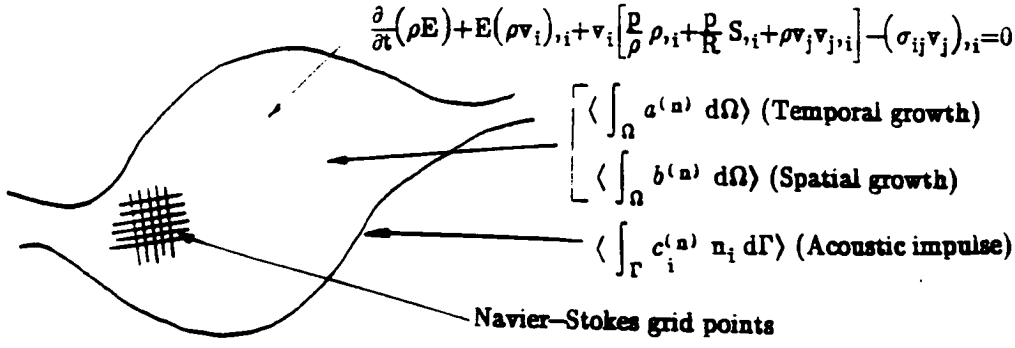

(a) Concept of ECI method

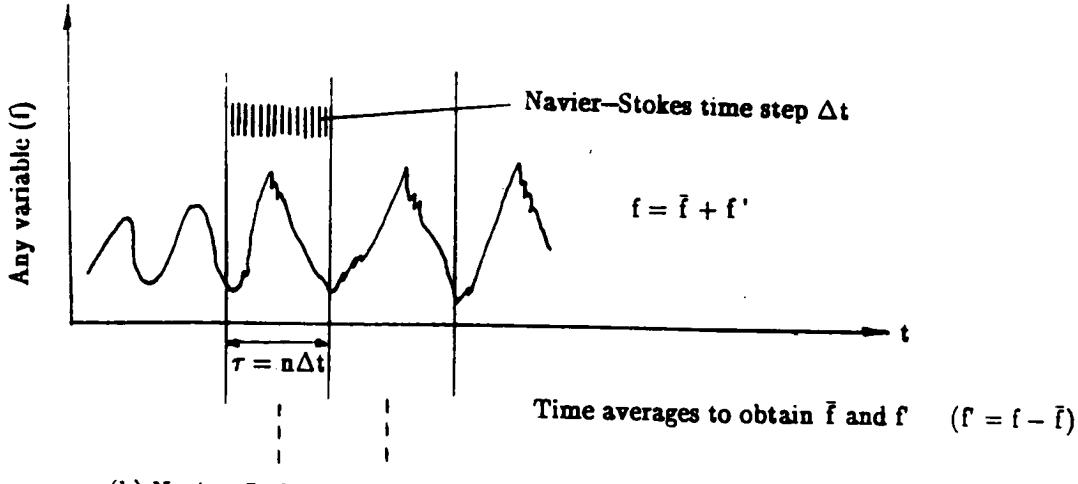

(b) Navier–Stokes solutions with initial oscillatory boundary conditions

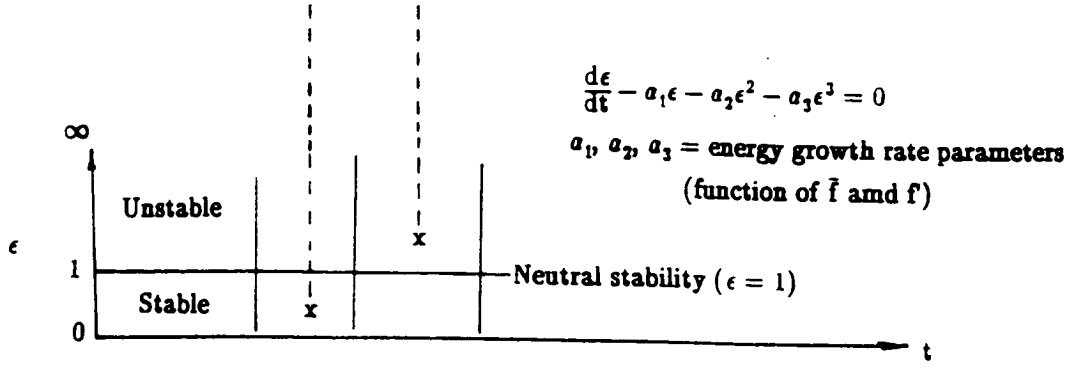

(c) Energy growth factor (ϵ)

Fig. 1 Schematic overview of ECI method

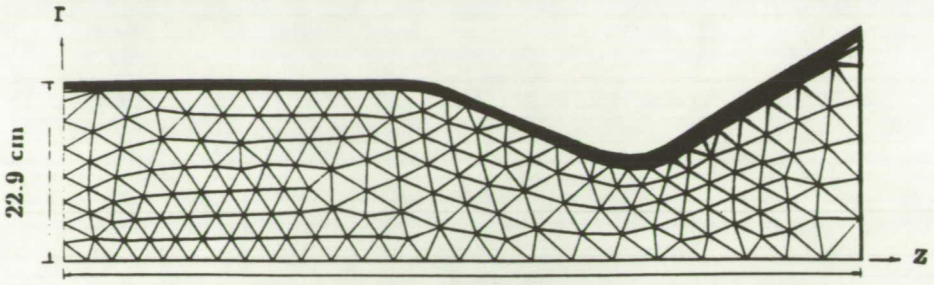

(a) Discretised geometry, 965 elements, 528 nodes

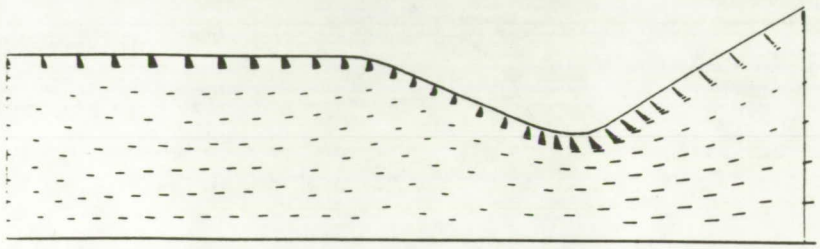

(b) Velocity field, 1 mm = 105 m/s

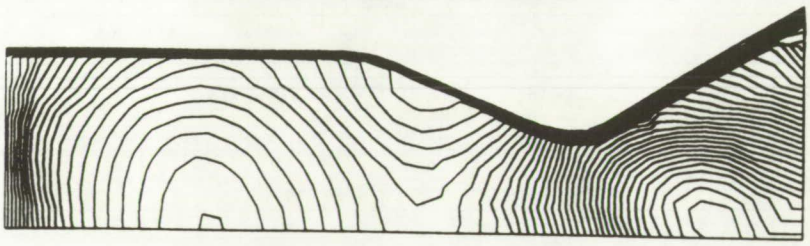

(c) Mach number contours, max = 1.6, min = 1.6, incr = 0.032

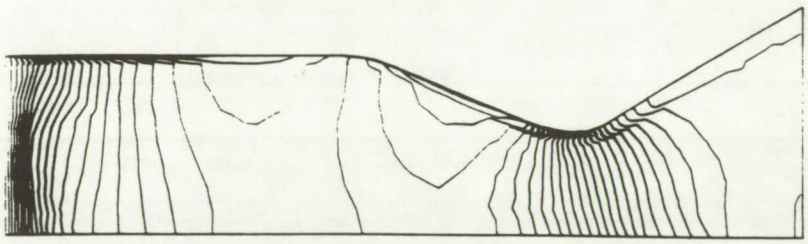

(d) Pressure contours, max = 3000 psi, min = 230 psi, incr = 53 psi

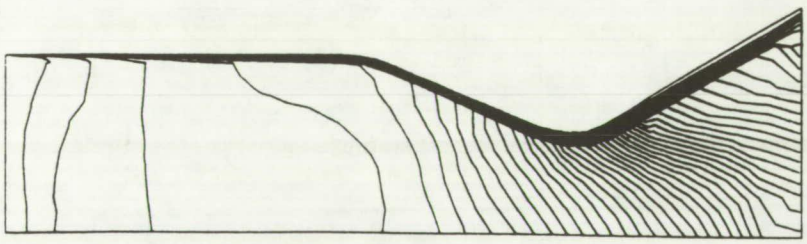

(e) Temperature contours, max = 3656.33° K, min = 8.26° K, incr = 72.96° K

Fig. 2 **Steady state laminar nonreacting flow without disturbances. M (inlet) = 0.2, Re = 66,000, $\mu = 0.23$ kg/m²/s, $\gamma = 1.2$, $\bar{p} = 3000$ psi, $\rho = 55.8$ kg/m³, T = 3656.33° K**

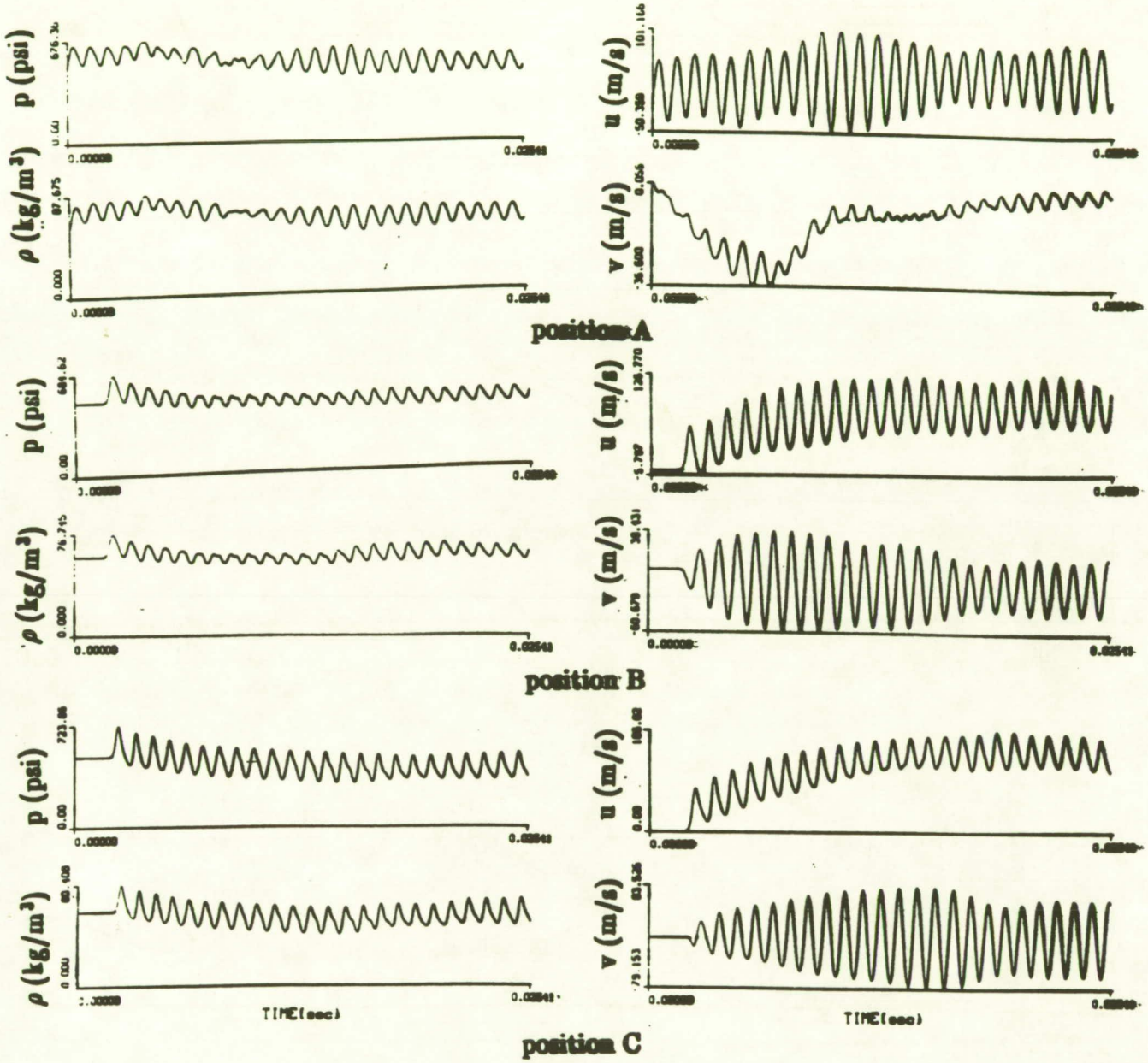

Fig. 3 Waveforms for transient laminar nonreacting flow with disturbances. Pressure, density, axial velocity, and radial velocity vs time at various positions. Position A (1.8, 11.43 cm), position B (31.75, 11.45 cm), position C (63.5, 6.55 cm)

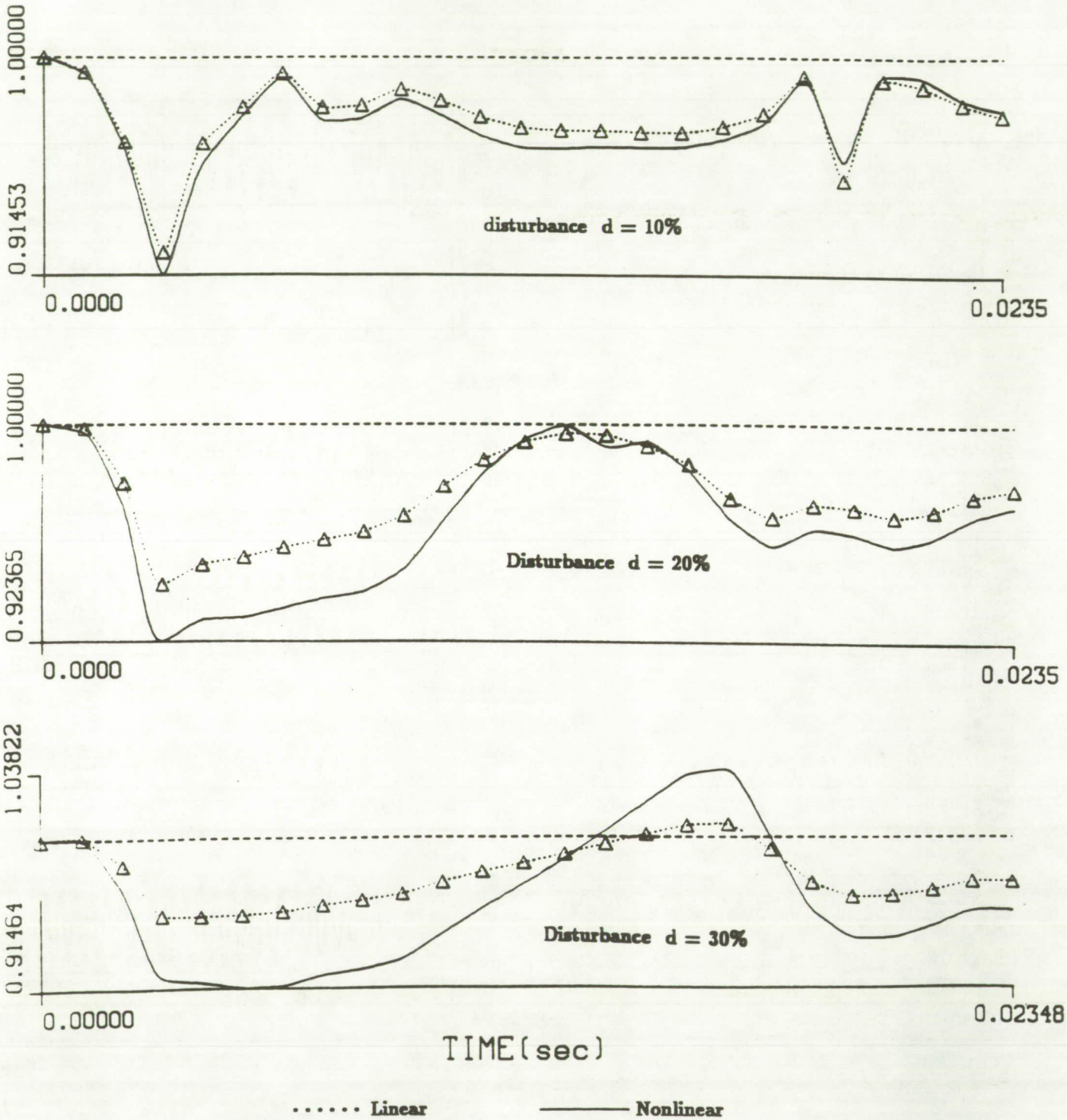

Fig. 4 Energy growth factor vs time, transient laminar flow with disturbances, $\bar{p}$ = 500 psi, f (inlet) = 1022 Hz, M (inlet) = 0.2

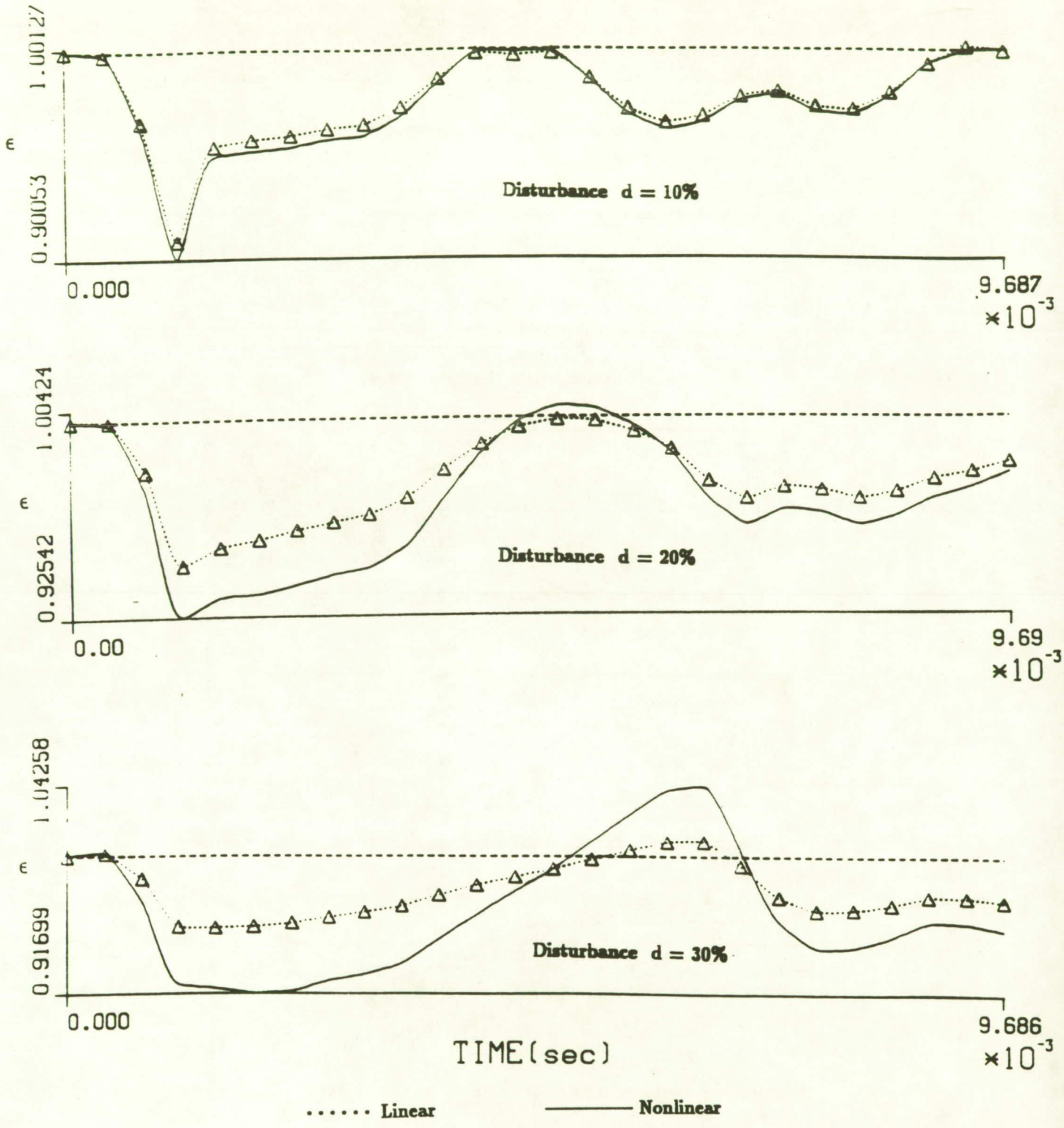

Fig. 5 Energy growth factor vs time, transient laminar flow with disturbances, $\bar{p}$ = 3000 psi, f (inlet) = 1022 Hz, M (inlet) = 0.2

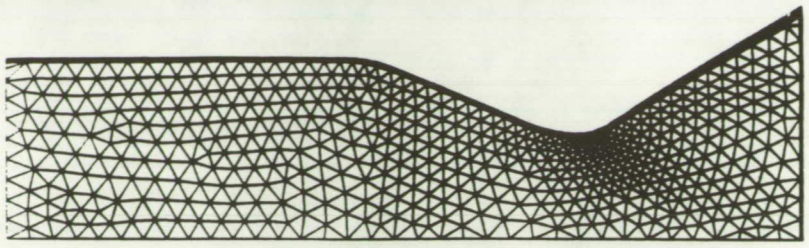

(a) Discretised geometry, 2688 elements, 1416 nodes

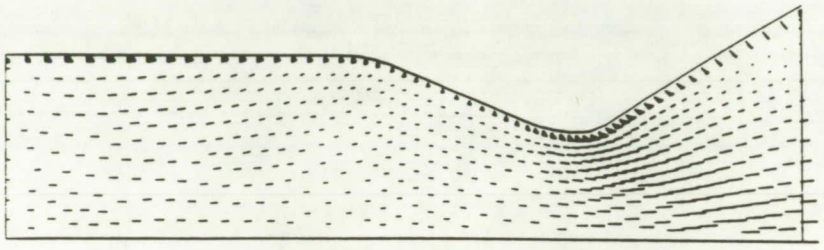

(b) Velocity field, 1 mm = 105 m/s

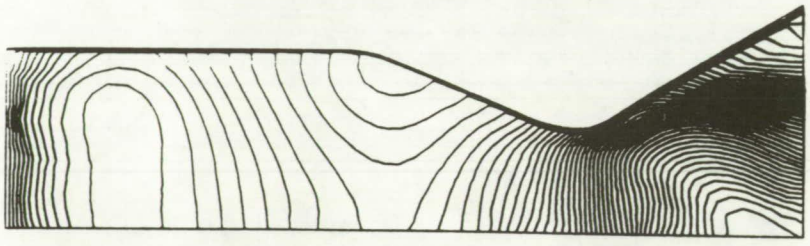

(c) Mach number contours, max = 2.2, min = 0, incr = 0.044

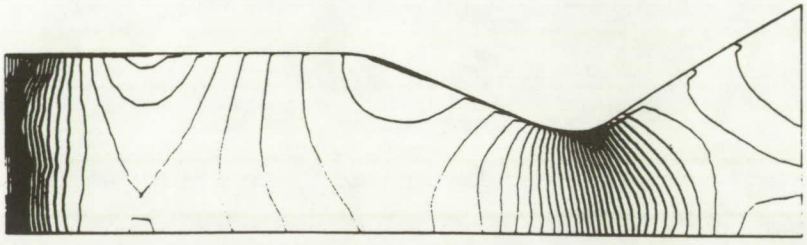

(d) Pressure contours, max = 3000 psi, min = 227 psi, incr = 54 psi

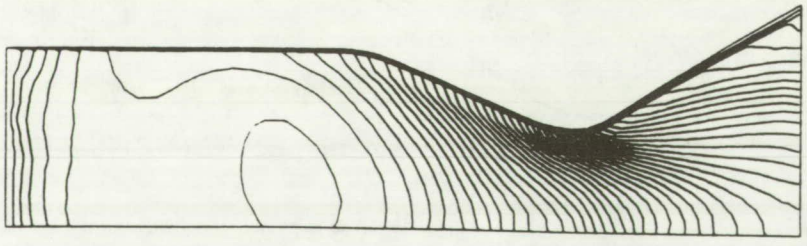

(e) Temperature contours, max = 3656.33° K, min = 15.45° K, incr = 72.82° K

Fig. 6 Steady state turbulent nonreacting flow without disturbances. M (inlet) = 0.2, Re = 500,000, $\mu = 1.737$ kg/m^2/s, $\gamma = 1.2$, $\bar{p} = 3000$ psi, $\rho = 55.8$ kg/m^3, T = 3656.33° K

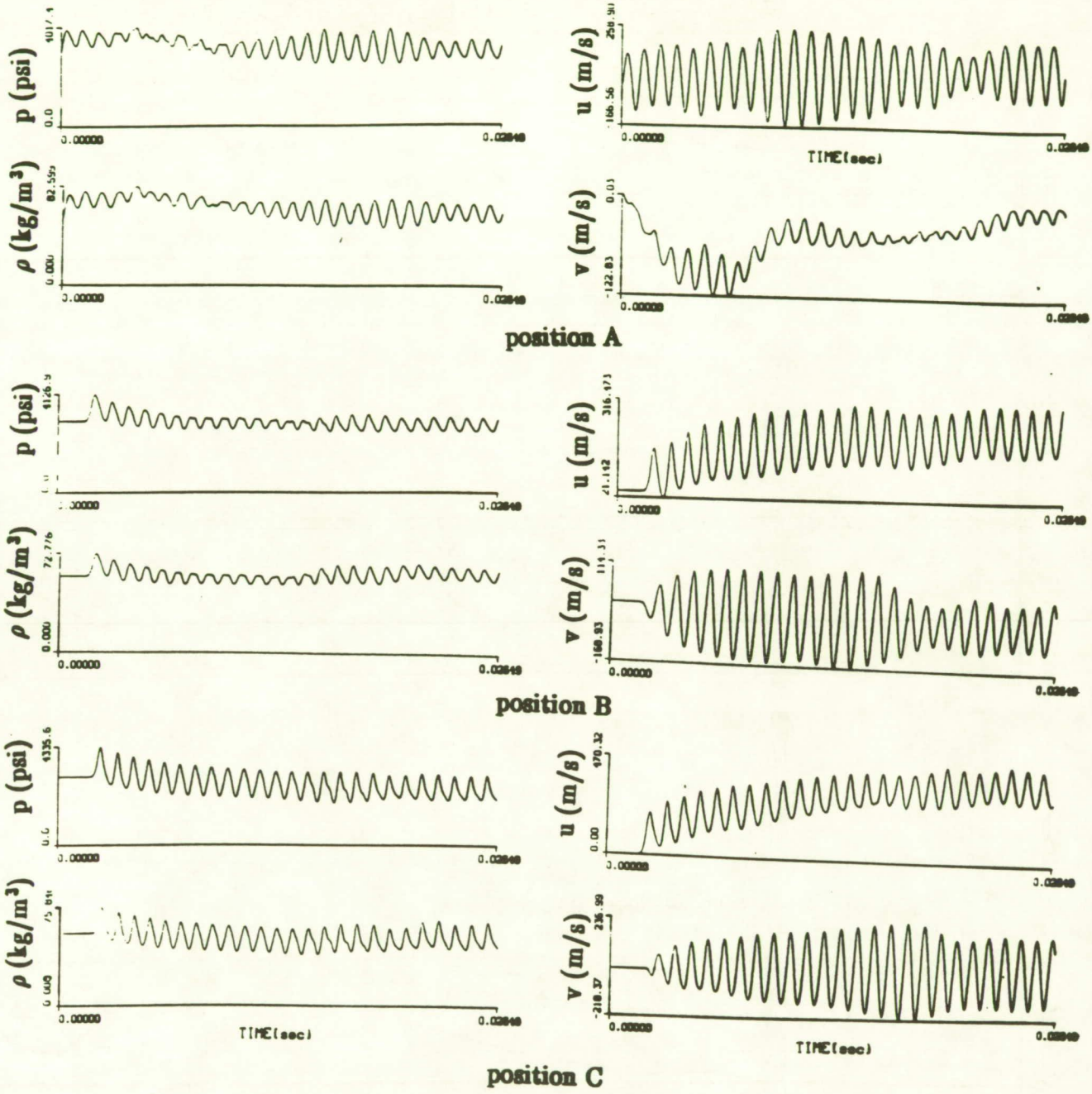

Fig. 7 Wave forms for transient turbulent flow with disturbances, pressure, density, axial velocity and radial velocity vs time at various positions. Position A (1.8, 11.43 cm), Position B (31.75, 11.45 cm), Position C (63.5, 6.55 cm)

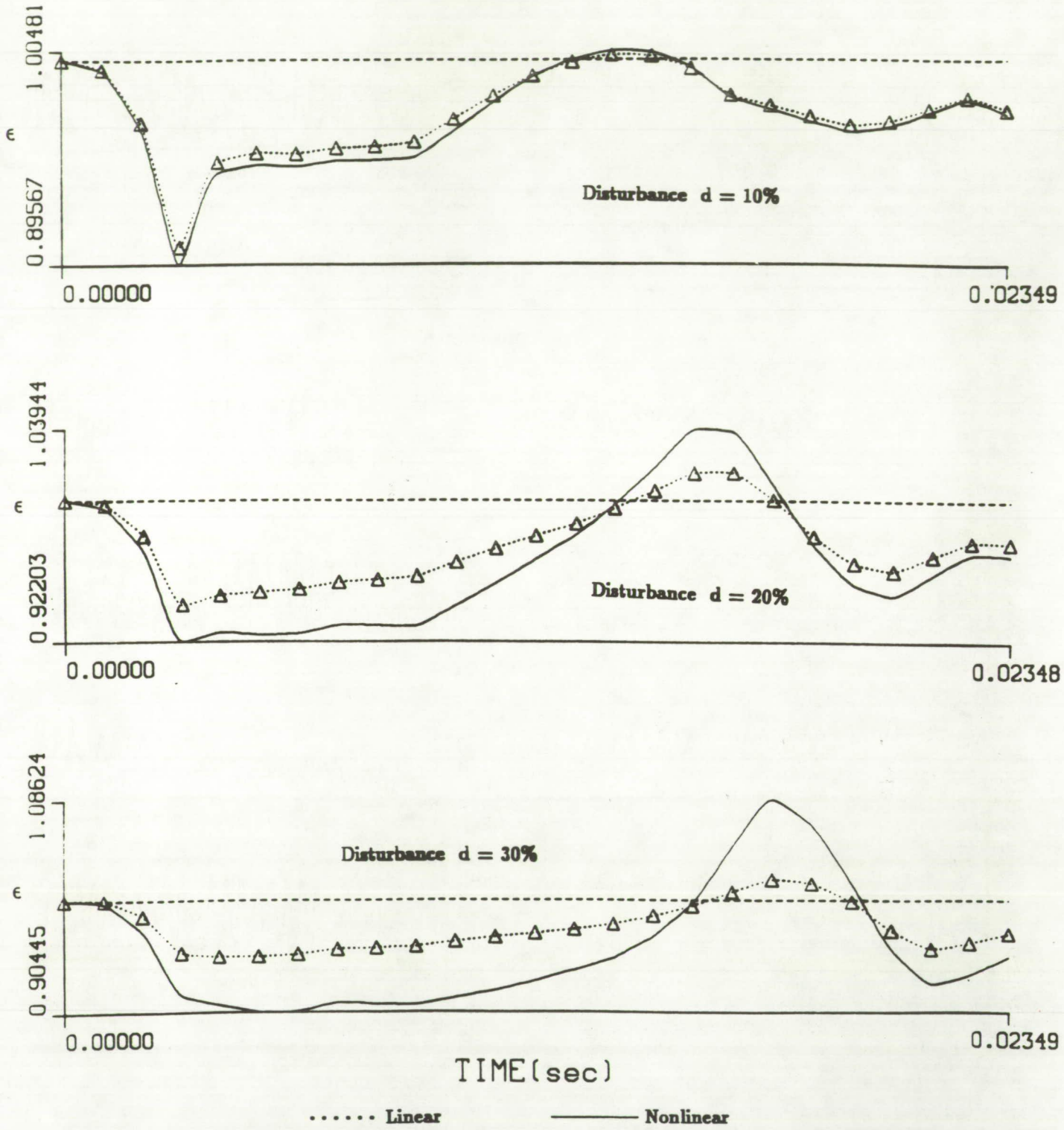

Fig. 8 **Energy growth factor vs time, transient turbulent flow with disturbances, $\bar{p}$ = 500 psi, f (inlet) = 1022 Hz, M (inlet) = 0.2**

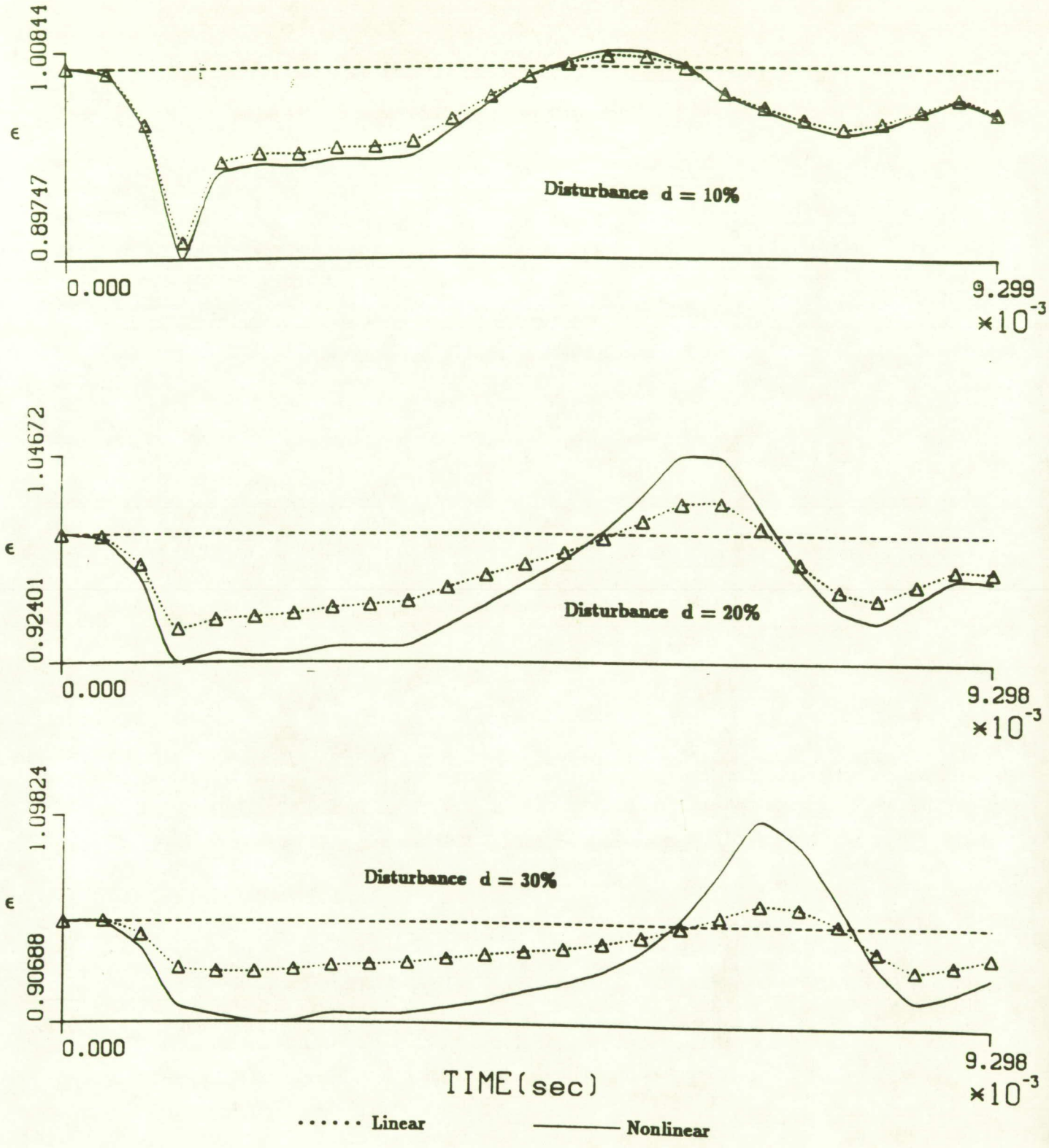

Fig. 9 Energy growth factor vs time, transient turbulent flow with disturbances, $\bar{p}$ = 3000 psi, f (inlet) = 1022 Hz, M (inlet) = 0.2

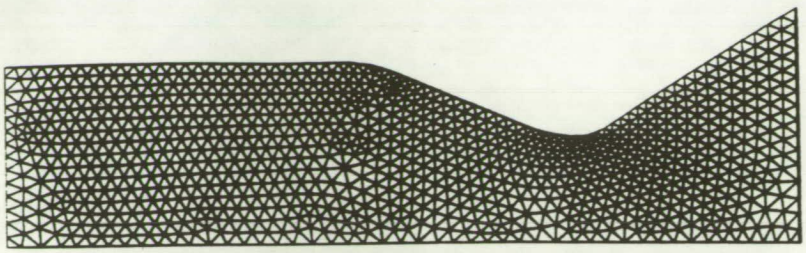

(a) Discretised geometry, 1580 elements, 844 nodes

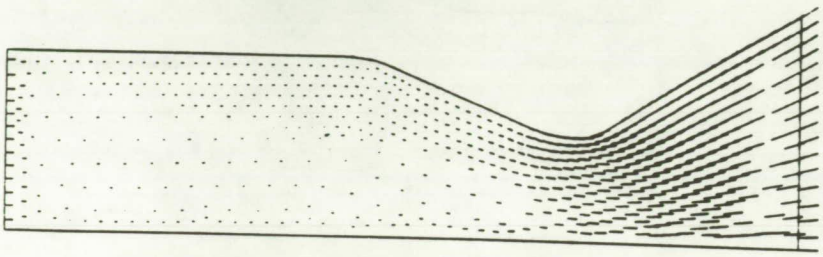

(b) Velocity field, 1 mm = 262 m/s

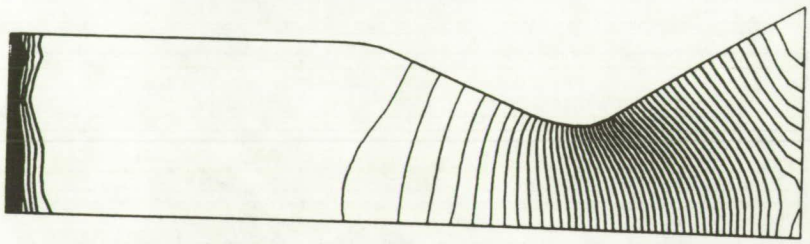

(c) Mach number contours, max = 4.8, min = 0.33, incr = 0.089

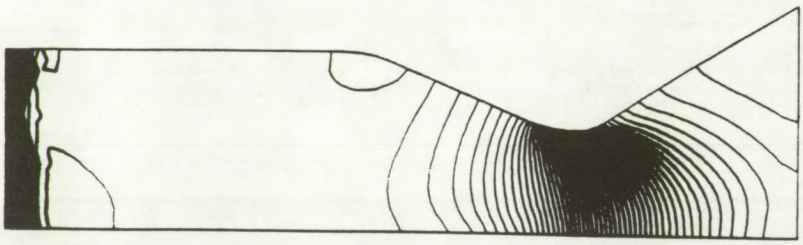

(d) Pressure contours, max = 1897 psi, min = 46 psi, incr = 37 psi

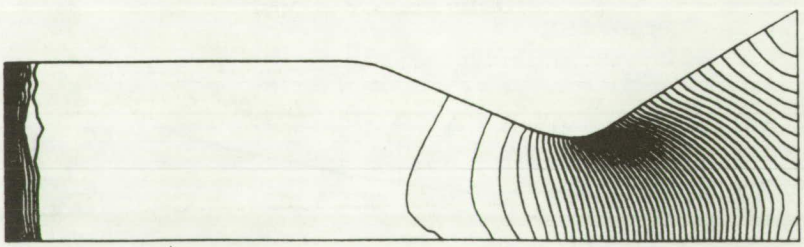

(e) Temperature contours, max = 635.1° K, min = 260.2° K, incr = 7.5° K

Fig 10 Steady state chemically reacting flow without disturbances, inlet velocity = 500 m/s, Re = 66,000, $\mu = 0$, $\gamma = 1.413$, $\bar{p} = 500$ psi, $\rho = 40.08$ kg/m^3, T = 500° K, inlet mass fraction $H_2 = 0.111$, $O_2 = 0.889$

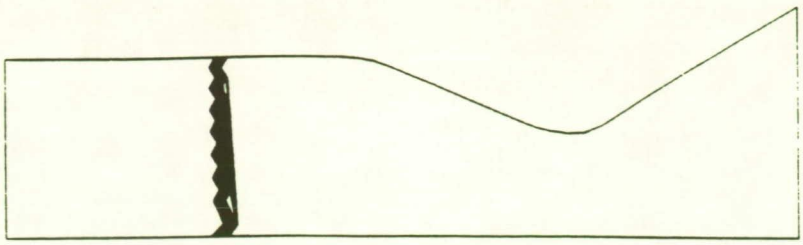

(a) H_2 contours, max = 0.111, min = 0.11, incr = 0.8×10^{-5}

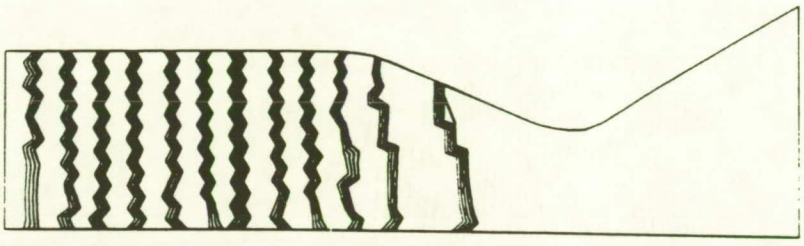

(b) O_2 contours, max = 0.889, min = 0.884, incr = 0.96×10^{-4}

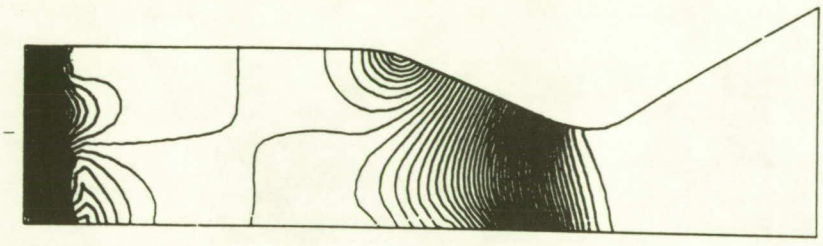

(c) H contours, max = 0.145×10^{-14}, min = 0, incr = 2.89×10^{-16}

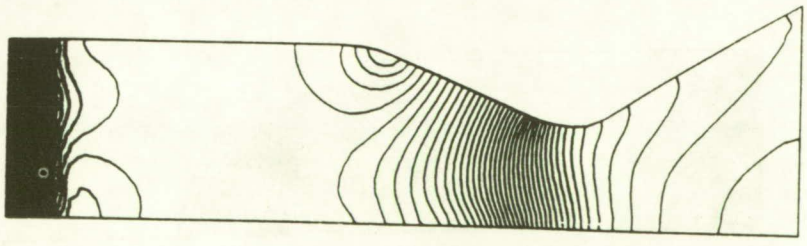

(d) HO_2 contours, max = 0.46×10^{-5}, min = 0, incr = 0.92×10^{-7}

Fig 11 Distributions of various chemical species at steady state without disturbances

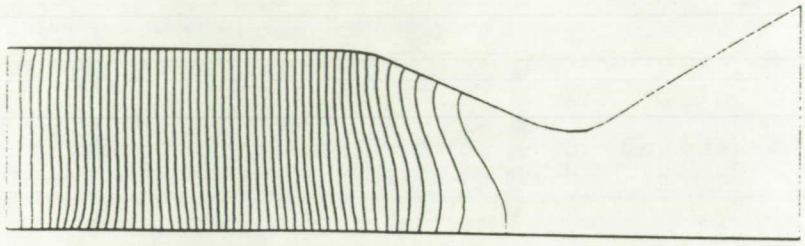

(e) H_2O contours, max = 0.0056, min = 0, incr = 0.00011

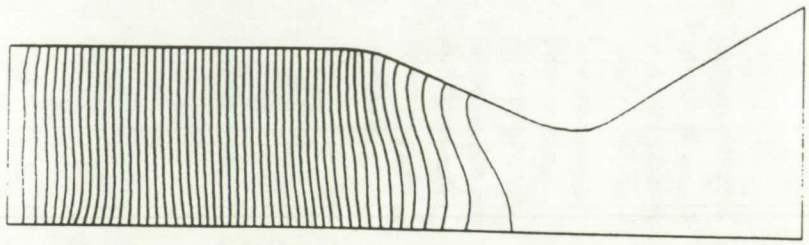

(f) H_2O_2 contours, max = 0.412×10^{-3}, min = 0, incr = 0.82×10^{-5}

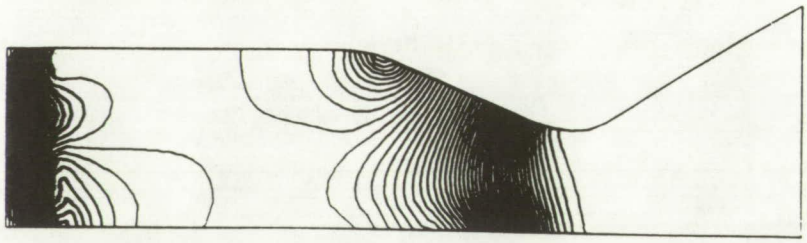

(g) O contours, max = 0.1139×10^{-11}, min = 0, incr = 0.22×10^{-13}

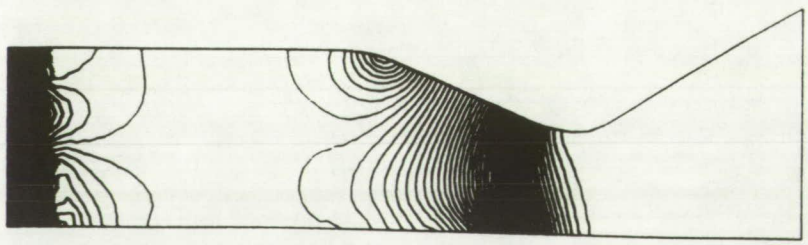

(h) OH contours, max = 0.5817×10^{-13}, min = 0, incr = 0.12×10^{-14}

Fig 11 Distributions of various chemical species at steady state without disturbances, continued.

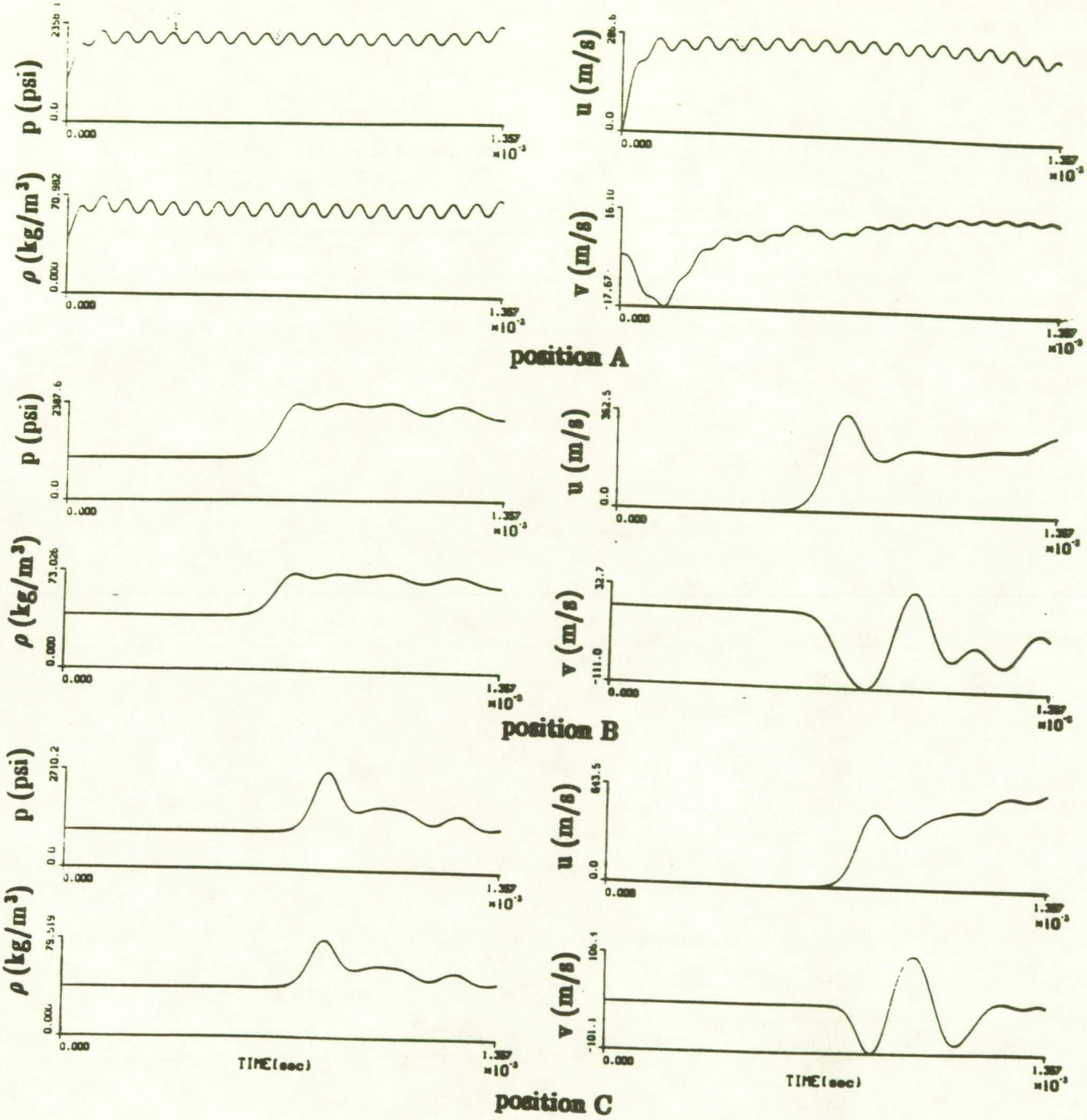

Fig 12 **Wave forms for transient chemically reacting flow with disturbances, pressure, density, axial velocity and radial velocity vs time at various positions. Position A (1.8, 11.43 cm), Position B (31.75, 11.45 cm), Position C (63.5, 6.55 cm)**

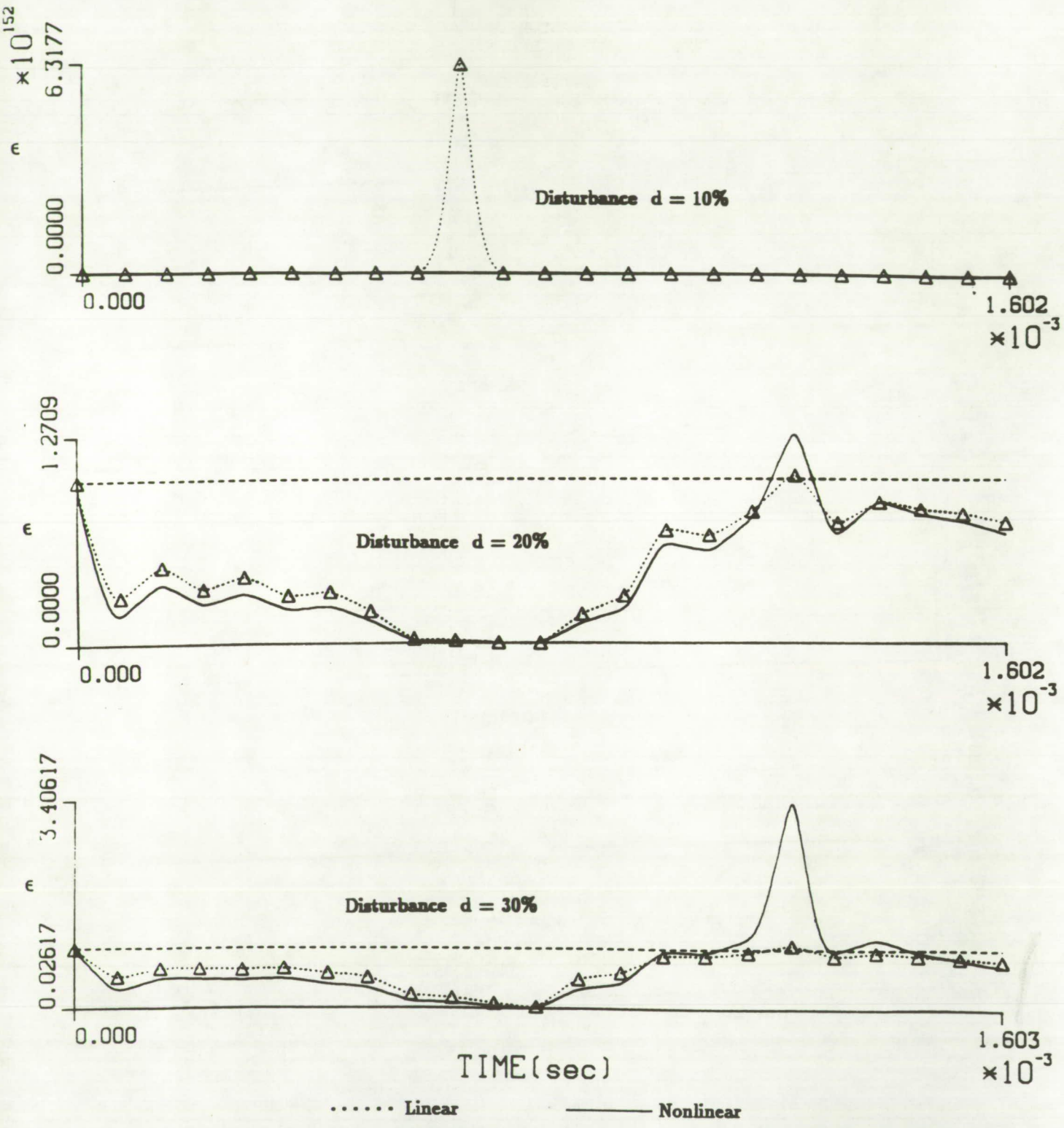

Fig 13 Energy growth factor vs time, transient chemically reacting laminar flow with disturbances, $\bar{p}$ = 500 psi, f (inlet) = 5583 Hz, inlet velocity = 500 m/s